

10

DAAG-80-0217

# RETRIEVED SIGNATURES FROM ATMOSPHERIC CLOUDS

Alan C. Stanton  
David C. Robertson

Aerodyne Research, Inc.  
Bedford Research Park  
Crosby Drive  
Bedford, Massachusetts 01730

May 1980

Scientific Report No. 3

Approved for public release; distribution unlimited.

DTIC  
ELECTRONIC  
JAN 14 1983  
H

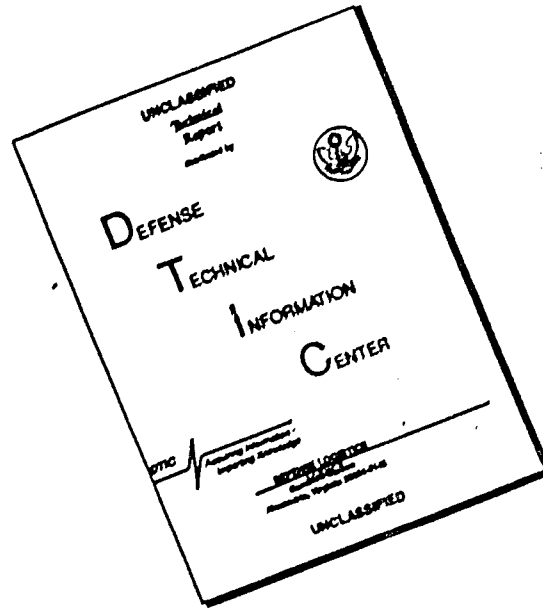
ADA123404

AIR FORCE GEOPHYSICS LABORATORY  
AIR FORCE SYSTEMS COMMAND  
UNITED STATES AIR FORCE  
HANSCOM AFB, MASSACHUSETTS 01731

DTIC FILE COPY

88 01 14 006

# DISCLAIMER NOTICE



THIS DOCUMENT IS BEST QUALITY AVAILABLE. THE COPY FURNISHED TO DTIC CONTAINED A SIGNIFICANT NUMBER OF PAGES WHICH DO NOT REPRODUCE LEGIBLY.

UNCLASSIFIED

SECURITY CLASSIFICATION OF THIS PAGE (When Data Entered)

REPORT DOCUMENTATION PAGE		READ INSTRUCTIONS BEFORE COMPLETING FORM
1. REPORT NUMBER AFGL-TR-80-0217	2. GOVT ACCESSION NO. A12 3404	3. RECIPIENT'S CATALOG NUMBER BAM 10
4. TITLE (and Subtitle)  INFRARED SIGNATURES FROM ATMOSPHERIC CLOUDS	5. TYPE OF REPORT & PERIOD COVERED Scientific Report No. 3 (March 1979-May 1980)	
	6. PERFORMING ORG. REPORT NUMBER ARI-RR-190	
7. AUTHOR(s) Alan C. Stanton and David C. Robertson	8. CONTRACT OR GRANT NUMBER(s) F19628-78-C-0145	
9. PERFORMING ORGANIZATION NAME AND ADDRESS Aerodyne Research, Inc. Bedford Research Park, Crosby Drive Bedford, MA 01730	10. PROGRAM ELEMENT, PROJECT, TASK AREA & WORK UNIT NUMBERS 63424F 212303AI	
11. CONTROLLING OFFICE NAME AND ADDRESS Air Force Geophysics Laboratory Hanscom AFB, Massachusetts Monitor: Albert McIntyre/OP	12. REPORT DATE May 1980	
	13. NUMBER OF PAGES 65	
14. MONITORING AGENCY NAME & ADDRESS (if different from Controlling Office)	15. SECURITY CLASS. (of this report) UNCLASSIFIED	
	15a. DECLASSIFICATION/DOWNGRADING SCHEDULE	
16. DISTRIBUTION STATEMENT (of this Report)  Approved for public release; distribution unlimited.		
17. DISTRIBUTION STATEMENT (of the abstract entered in Block 20, if different from Report)		
18. SUPPLEMENTARY NOTES		
19. KEY WORDS (Continue on reverse side if necessary and identify by block number)		
20. ABSTRACT (Continue on reverse side if necessary and identify by block number) (U) Clouds are an important source of variations in the IR background radiation as detected by satellite surveillance systems, because clouds absorb and scatter solar radiation and have a blackbody temperature different from that of the earth's surface. In the present study, a model which describes the scattering, absorption, and emission of radiation by atmospheric water or ice clouds is synthesized from previous works on the scattering of solar radiation. The cloud model is combined with the LOWTRAN atmospheric		

DD FORM 1473

1 JAN 73

EDITION OF 1 NOV 65 IS OBSOLETE  
S/N 0102-LF-014-6601

UNCLASSIFIED

SECURITY CLASSIFICATION OF THIS PAGE (When Data Entered)

UNCLASSIFIED

SECURITY CLASSIFICATION OF THIS PAGE (When Data Entered)

Abstract (Cont.)

transmission model and is used to predict the apparent spectral radiance from scenes containing clouds as detected by a downward-looking observer. The effects of solar scatter, thermal emission, transmitted upwelling radiation, and atmospheric attenuation are included. Calculations using the model have been compared with infrared cloud data from several sources, including radiometer data from the BMM (Balloon Altitude Mosaic Measurements) Program. These analyses suggest that low altitude cumulus clouds are not an important source of background signal variations in the 2.7-3.1  $\mu\text{m}$  region. The BMM data and model calculations indicate that high altitude cirrus clouds can cause large spatial variations in the background signal in this wavelength region, due to enhanced solar scatter in the wings of the water vapor absorption bands. Comparisons illustrating the spectral and directional characteristics of IR cloud signals are presented.

S/N 0102-LF-014-6601

UNCLASSIFIED

SECURITY CLASSIFICATION OF THIS PAGE (When Data Entered)

# TABLE OF CONTENTS

<u>Section</u>		<u>Page</u>
	ACKNOWLEDGMENTS .....	7
1	INTRODUCTION .....	9
2	CLOUD MODEL .....	13
	2.1 Viewing Scenario.....	13
	2.2 Cloud Model .....	15
	2.2.1 Single Scattering.....	18
	2.2.2 Multiple Scattering .....	23
	2.3 Two-Stream Model .....	24
	2.4 Implementation of the Cloud Model.....	29
	2.5 Other Cloud Modeling Work .....	33
3	COMPARISONS WITH CLOUD SPECTRAL DATA .....	35
	3.1 2.7 $\mu\text{m}$ $\text{H}_2\text{O}/\text{CO}_2$ Band .....	35
	3.2 Comparisons to AFGL Data .....	38
4	COMPARISON OF MODEL PREDICTIONS WITH BMM DATA .....	43
	4.1 Mountain Terrain Background (Clear Air).....	43
	4.2 Elevation Scan: Desert/Mountain Background with Possible Cirrus Cloud .....	47
	4.3 Cumulus Clouds (Low Altitude).....	54
5	SUMMARY .....	61
	REFERENCES .....	63

DTIC  
COPY  
NUMBER 2

Accession For	
NTIS GRA&I	<input checked="" type="checkbox"/>
DTIC TAB	<input type="checkbox"/>
Unannounced	<input type="checkbox"/>
Justification	
By _____	
Distribution/	
Availability Codes	
Dist	Avail and/or Special
A	



List of Illustrations (Cont.)

<u>Figure</u>		<u>Page</u>
14	Comparison of Apparent Cloud Spectral Radiance (at observer altitude) and Clear-Air Background Radiance for two cloud altitudes .....	52
15	Radiance-Time Profile for An Azimuthal Scan Over Cumulus Clouds .....	55
16	Radiance-Time Profile for a Cumulus Cloud - Clear-Air Background (Staring Mode) .....	59

## LIST OF TABLES

<u>Table</u>		<u>Page</u>
1	Comparison of Single Scatter Phase Functions in the Forward Scattering Peak (Scattering Angle = $10^{\circ}$ ) .....	41
2	Baseline Input Parameters for Background Radiance Calculations (Scene Ic and Scene Id) .....	44
3	Baseline Radiance Calculation for Scene I .....	45
4	Calculated In-Band Radiance for Several Atmospheric Profiles.....	46
5	Fraction of Calculated In-Band Radiance Due to Reflected Solar Radiation .....	46
6	Calculated In-Band Radiance (BAMM Filter 1) For a Background Scene Including An Ice Cloud at 50,000 ft Altitude (Cloud Thickness = 2 km).....	51
7	Input Parameters for Low Altitude Cumulus Cloud Calculations (BAMM Scene II) .....	56
8	Calculated Radiance Levels (In-Band) for Background Features in BAMM Azimuth Scans (Scene II).....	57

## ACKNOWLEDGMENTS

The support of Dr. Randall Murphy and Mr. Al McIntyre of the Air Force Geophysics Laboratory is gratefully acknowledged. Technical discussions with Dr. Murphy and Dr. Michael McElroy, Director of the Center for Earth and Planetary Physics, Harvard University, resulted in important contributions to this work. The authors especially wish to thank Ms. Margot Tollefson of Aerodyne Research, Inc., who performed most of the calculations discussed in this report.

## 1. INTRODUCTION

An important element in our National Defense is the development of satellite based surveillance systems to monitor the appearance and progress of any potential threat. The infrared (IR) spectral region for detection systems shows good promise for being able to detect various targets at different altitudes. In support of continued development of IR detection systems, it is necessary to fully specify and understand the upwelling IR radiance from the earth-atmosphere scene within a given field-of-view (FOV). Detecting the radiation from a target requires that not only the target intensity but also the spectral and spatial structure of the background be fully understood. Onboard processing capabilities must be able to distinguish variations in the upwelling radiation due to various target signatures from variations arising from background spatial and temporal features. Thus, any detection system must be designed to know and interpret the variances in the levels of IR radiation from a FOV scene; these variations include the temporal, spatial, and spectral structure of the radiation.

Important inputs to the design of successful detection systems are the magnitude and variations in the radiance from various sources. This knowledge will aid in developing data processing algorithms to distinguish radiation signatures of clouds and other surface features from those of the target. Spectral, spatial, and temporal data combined with phenomenological analyses will provide the information required for systems design. The data and analysis will address such questions as fluctuation intensities, signal to noise, solar scattering effects, FOV stability, and effects of atmospheric turbulence. In many cases, these data are best summarized in validated calculational models which quantitatively describe the important physical phenomena and are convenient for use by the systems designer.

Clouds will be a significant source of variations in the IR radiation for any system viewing the earth's surface, as they cover approximately 30 percent of the earth surface at any given time. Clouds affect a satellite system's ability to detect a target from space in several different ways:

- Obscuration: Clouds occult the sensor's view of the target.
- Background Signal Variations: Clouds change the background radiance level in a FOV because they scatter solar radiation and have a blackbody temperature different from that of the earth surface.
- Signal Degradation: Optically thin clouds modulate the target and background signals by reducing their intensity. Additionally, high altitude cirrus will also scatter solar radiation into the line of sight.

The Balloon Airborne Mosaic Measurements (BAMM) Program is tasked to make extensive measurements of the earth surface as would be seen from a high altitude, down-looking system. Since the BAMM platform is at an altitude of 30 km, these data include low and high altitude clouds, as well as earth surface features such as land-water interfaces. In support of this program Aerodyne Research has developed a general calculational model for the upwelling earth radiance, based on the AFGL LOWTRAN code for atmospheric transmittance and radiation. The calculational model for scattering and emission of radiation by a cloud uses an approximate solution to the radiative transfer equation, which incorporates multiple scattering effects. The purpose of the model is to enable quick calculations of the upwelling atmospheric radiation for arbitrary sun-viewer-cloud-background viewing scenarios. The primary motivation for the modeling approach is to develop a calculationally flexible model which captures the salient features of the IR background scene. Therefore, the model is based on the LOWTRAN atmospheric transmission code and a simplified diffusion scattering model for describing multiple scattering effects within a cloud. In this report the model is compared to radiance data for clouds viewed from the BAMM and other measurement platforms.

Section 2 of the report discusses modeling of the physical processes for scattering, absorption, and emission of radiation within a cloud. The important assumptions which are made for describing the radiation transfer are identified. This section also shows the application of a simple two-stream radiation transfer model for the radiation field and includes a detailed description of the formalism for calculating the radiation from a cloud. In Section 3, we compare the model predictions to data taken by the Arthur D. Little Company and by the Air Force Geophysics Laboratory Flying Laboratory (KC135A). In Section 4, the model is compared to data taken under the BAMB Program. In Section 5, the results are summarized and some implications for downward looking systems are indicated.

## 2. CLOUD MODEL

### 2.1 Viewing Scenario

When viewing the earth background from a high altitude satellite or balloon platform, the upwelling IR radiation can be described in terms of two signature elements: earth-atmosphere thermal emission and solar radiation scattered into the instrument line of sight. The intensity of the measured signal is a sensitive function of the sun-earth-observer viewing geometry. Clouds complicate the description of the radiation field by attenuating radiation from the earth surface and strongly scattering solar radiation. The schematic shown in Fig. 1 illustrates the viewing scenario and indicates the important IR phenomena which must be incorporated when modeling scenes that contain clouds. The cloud model described in these sections is designed to calculate the upwelling IR radiation for a wide range of viewing scenarios which include both optically thin and thick clouds. When validated against the BMM data, the model can be used as the basis for systems design calculations. The purpose of the model is to give reasonable results with sufficient flexibility for incorporating different parameters such as cloud type and altitude, atmospheric conditions, solar position, observer altitude, and background conditions. Since the amount of solar radiation scattered by clouds varies considerably, the model must include the effects of important microphysical cloud properties such as particle size, distribution, and scattering properties. Additionally, clouds can be composed of either water droplets or ice particles, or a mixture of the two. The present model is designed to incorporate these features and allow the user to select from a range of cloud properties.

## BAMM VIEWING GEOMETRY

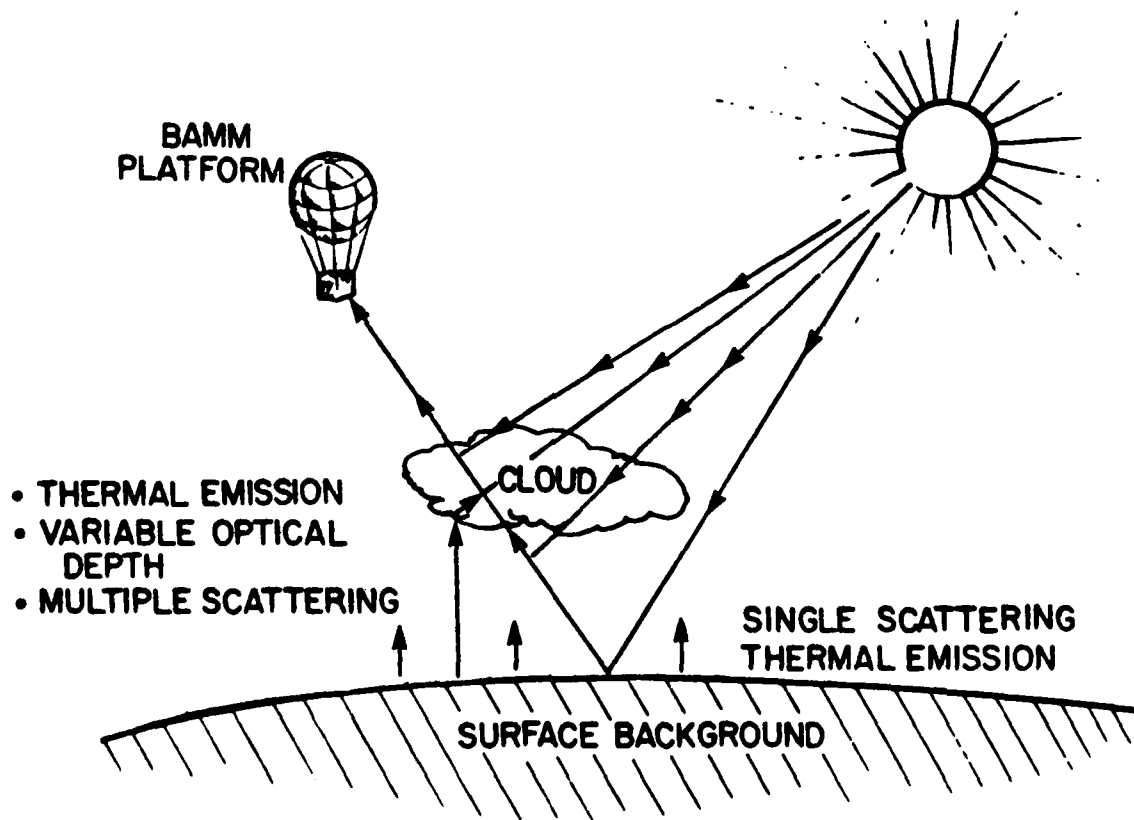


Figure 1. Schematic Showing Field of View Elements Which Contribute to the Upwelling Infrared Radiation Observed from the BAMM Platform.

## 2.2 Cloud Model

Considerable theoretical and empirical effort has been expended in developing calculational models which are capable of predicting the upwelling radiation field in the presence of clouds. The major thrust of these efforts has been to develop global and local climatological models for predicting how clouds affect the planetary albedo, the surface cooling rate, and the upwelling radiance data taken by meteorological satellites. The emphasis of these studies has been on predicting the net upward flux (the radiance integrated over wide bandpasses and the upper hemisphere). The Air Force interest in surveillance problems dictates that new effort be directed toward prediction of directional radiances (FOV observed by a satellite system) within narrow bandpasses (target identification by spectral signature).

The calculational models can be divided into two categories; exact but computationally slow models and approximate, computationally fast models. Because a satellite platform will view a large complicated earth scene that includes, in addition to clouds, surface features, surface vehicles, varying atmospheric conditions, changing sun-FOV background-observer geometry, and moving targets, the emphasis of the present modeling effort was placed on the faster calculational techniques. Comparisons to field data and to the detailed models will aid in validating the model and quantifying its limitations. Multiple scattering effects within a cloud are the most difficult to model; several of the techniques include the doubling method first suggested by van de Hulst,<sup>(1,2,3,4)</sup> Monte

---

<sup>1</sup>van de Hulst, H.C., "A New Look at Multiple Scattering," Institute for Space Studies Report, NASA, New York (1963).

<sup>2</sup>Hansen, James E. and Pollack, James B., "Near Infrared Scattering by Terrestrial Clouds," J. Atmo. Sci., 27, 266 (1970).

<sup>3</sup>Hansen, James E., "Exact and Approximate Solutions for Multiple Scattering by Hazy Atmospheres," J. Atmo. Sci., 26, 478 (1969).

<sup>4</sup>Welch, R. M. and Cox, S. K., "Absorption of Solar Radiation in Clouds; The Effect of Monomodal and Bimodal Size Distributions," Third Conference on Atmospheric Radiation, American Met. Soc. (1978).

Carlo calculations,<sup>(5,6)</sup> and multiple stream approaches.<sup>(7,8,9)</sup> The model outlined below is based on a two-stream (upward and downward radiance) approach that is a simpler form of the multiple stream models. This approach draws on results from previous efforts in forming a calculational model which applies with reasonable accuracy to different cloud altitudes, types and thicknesses.

Clouds strongly scatter radiation in the infrared because of their high density of aerosols (either liquid H<sub>2</sub>O or ice crystals). Low altitude cumulus clouds are usually composed of liquid H<sub>2</sub>O or a liquid-ice mixture.<sup>(10,11)</sup> At higher altitudes with their colder temperatures, cloud droplets are almost exclusively ice.<sup>(8)</sup> Thin, high altitude, cirrus clouds transmit much of the upwelling radiation from below, while scattering significant amounts of the impinging solar radiation. This effect can lead to enhanced IR signals in the shorter wavelength regions, while maintaining information about signals arising in the lower altitudes.

---

<sup>5</sup> Davies, Roger, "The Three-Dimensional Transfer of Solar Radiation in Clouds," Ph.D. Thesis, University of Wisconsin, Madison, Wisconsin (1976) and J. Atmo. Sci.

<sup>6</sup> McKee, T. B. and Cox, S. K., "Scattering of Visible Radiation by Finite Clouds," J. Atmo. Sci., 31, 1886 (1974).

<sup>7</sup> Liou, Kuo-Nan and Wittman, Gerald D., "Parameterization of the Radiative Properties of Clouds," J. Atmo. Sci., 36, 1261 (1979).

<sup>8</sup> Roewe, Douglas and Liou, Kuo-Nan, "Influence of Cirrus Clouds on the Infrared Cooling Rate in the Troposphere and Lower Stratosphere," J. Appl. Meteor., 17, 92 (1978).

<sup>9</sup> Harshvardhan, "Perturbation of the Zonal Radiation Balance by a Stratospheric Aerosol Layer," J. Atmo. Sci., 36, 1274 (1979).

<sup>10</sup> Pruppacher, Hans R. and Klett, James D., "Microphysics of Clouds and Precipitation," Reidel Publishing Co., Boston (1978).

<sup>11</sup> Kuhn, P.M. and Weickmann, H. K., "High Altitude Radiometric Measurements of Cirrus," J. Appl. Meteor., 8, 147.

The upwelling radiation described by the model is obtained by solving the generalized monochromatic equation of radiation transport,<sup>(12,13)</sup> which is:

$$\mu \frac{dI_{\nu}}{d\tau} = I_{\nu} - \frac{1}{4\pi} \int_{-1}^1 d\mu' \int_0^{2\pi} d\phi' p(\mu, \phi; \mu', \phi') I(\tau, \mu', \phi') - (1 - \omega_{\nu}) B_{\nu}(T) - \frac{F}{4} \exp(-\tau/\mu_0) p(\mu, \phi; -\mu_0, \phi_0) , \quad (1)$$

where the rate of change of spectral radiance  $I(\tau, \mu)$  at an optical depth  $\tau$  and zenith direction cosine  $\mu$  results from the contributions of the radiation elements on the right hand side. In order, these terms describe:

- Attenuation of the radiation due to absorption and scattering out of the observer's line of sight (LOS);
- Ambient radiation scattered into the LOS from all directions;
- Thermal emission from the cloud and/or atmosphere, and
- Radiation scattered into the observer's LOS from external sources.

The external source in the present problem is the solar irradiance. The upwelling radiation from the earth and atmosphere is included as a boundary condition for the lower edge of a cloud because it is a diffuse source term. Since the integro-differential equation cannot be solved in closed form, approximate solutions that describe the salient features must be developed. Before describing these approximate solutions to the radiative transfer equation, model approximations to the process of scattering by single particles are described and developed.

<sup>12</sup> Chandrasekhar, Radiative Transfer, Dover, New York (1950).

<sup>13</sup> McElroy, M.B., "The Composition of Planetary Atmospheres," J. Quant. Spectrosc. Radiat. Transfer, 11, 813 (1971).

### 2.2.1 Single Scattering

The single scattering event is described by the differential cross section for an incident photon to be scattered into an arbitrary direction. This cross-section is written as a phase function,  $P(\mu_s)$ , which is defined as

$$P(\mu_s) = \frac{1}{\sigma} \frac{d\sigma}{d\mu_s} \Big|_{\mu_s} \quad (2)$$

where  $\frac{d\sigma}{d\mu_s}$  is the differential cross section for a given particle size distribution<sup>s</sup>, and  $\mu_s$  is the cosine of the scattering angle. Scattering calculations based on Mie theory provide a good description of the scattering phase function for spherical particles.<sup>(14,15,16)</sup> The first step in these calculations is to determine the distribution of droplet sizes. Figures 2 and 3 give examples of the scattering phase function (calculated from Mie theory) for different particle size distributions.<sup>(2)</sup> Figure 2 shows the single scatter phase function for moderate and large mean particle sizes. The curves have been displaced vertically by factors of ten. The horizontal lines on the curves correspond to the point  $P(\theta) = 1$ . Figure 3 shows the single scatter albedo for spherical water and ice particles as reported by Hansen and Pollack.<sup>(2)</sup> Two different mean particle radii are shown, 2  $\mu\text{m}$  and 32  $\mu\text{m}$ . The particle size distributions are given by<sup>(17)</sup>

$$n(r) \propto r^6 \exp(-6r/r_m) \quad (3)$$

<sup>14</sup> Friedlander, S.K., Smoke, Dust and Haze, John Wiley and Sons, New York (1977).

<sup>15</sup> Zachor, A.S., Holzer, J.H., Smith, F.G., "IR Signatures Study," Honeywell Electro-Optics Center Report No. 7812-8, December 1978.

<sup>16</sup> Shettle, E. (Calculations reported in Zachor, et al., Ref. 15).

<sup>17</sup> Deirmendjian, "Scattering and Polarization Properties of Water Clouds and Hazes in the Visible and Infrared," Appl. Opt., 3, 187 (1964).

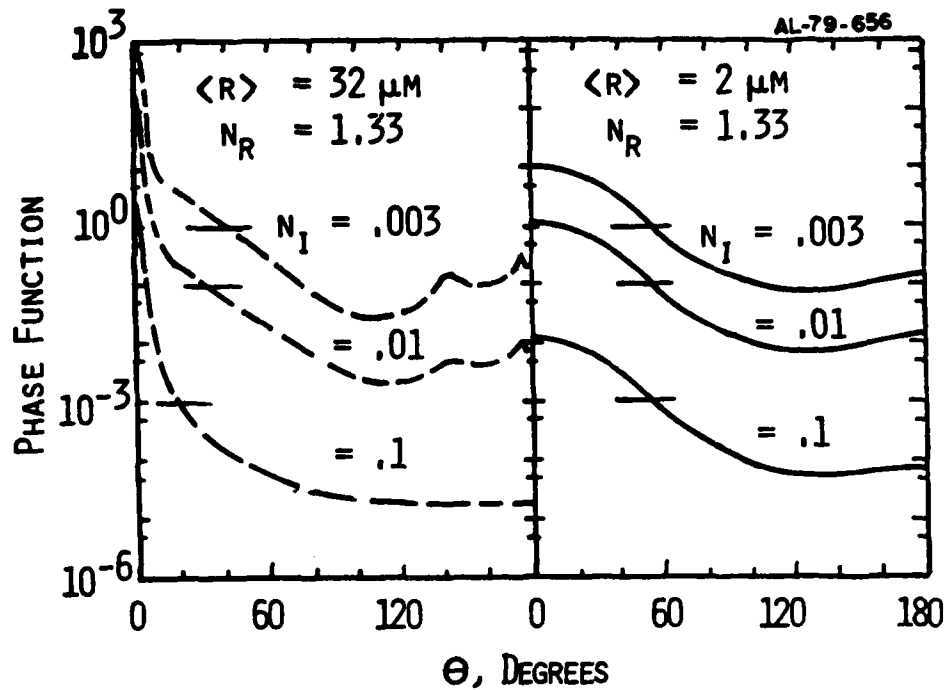


Figure 2. Single-Scattering Phase Function for Two Size Distributions of Spherical Particles Showing the Effect of Absorption. The Horizontal Lines Correspond to the Value 1.0. From Ref. (2).

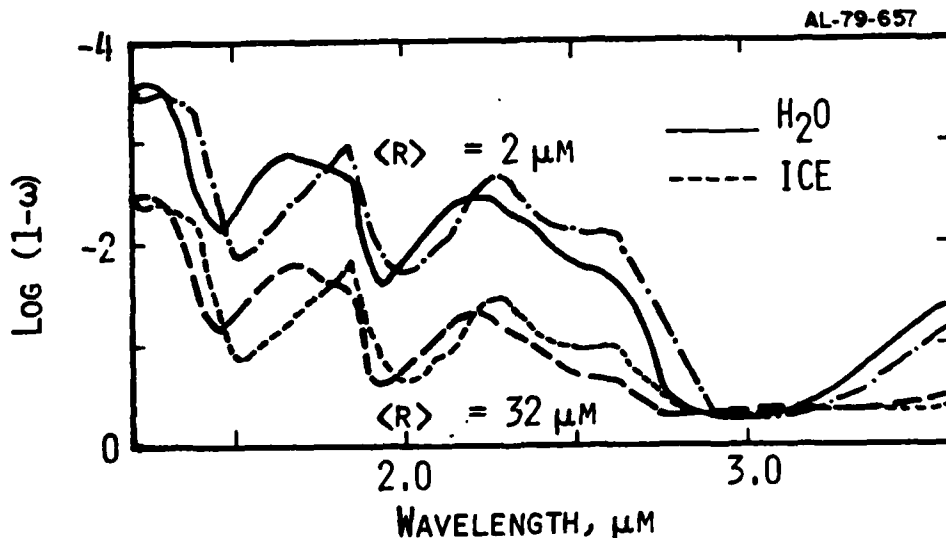


Figure 3. Comparison of the Single Scattering Albedo For Water Droplets and Spherical Ice Crystals at Two Different Mean Particle Radii. From Ref. (2).

where  $r_m$  is the mean particle radius. Since conventional Mie calculations strictly apply only for spherical particles, a basic assumption of virtually all cloud models is that the particles are spherical. Mie type calculations have been carried out for cylindrical particles, which are more representative of ice crystals.<sup>(18)</sup> Figure 4, which is taken from Liou's work,<sup>(18)</sup> indicates that the cylinders scatter a little more than the spheres and have less structure at larger scattering angles. The assumption of spherical particles is very good for water droplets but is less valid for ice crystals which are large (10-100  $\mu\text{m}$ ) and often hexagonal in shape. From these curves, one sees that the increase in the back scatter becomes weaker as the particle shapes become more asymmetric. Therefore, we have not made any attempt to include a back-scattered enhancement in the present model because higher altitude clouds contain ice crystals with their nonspherical shapes.

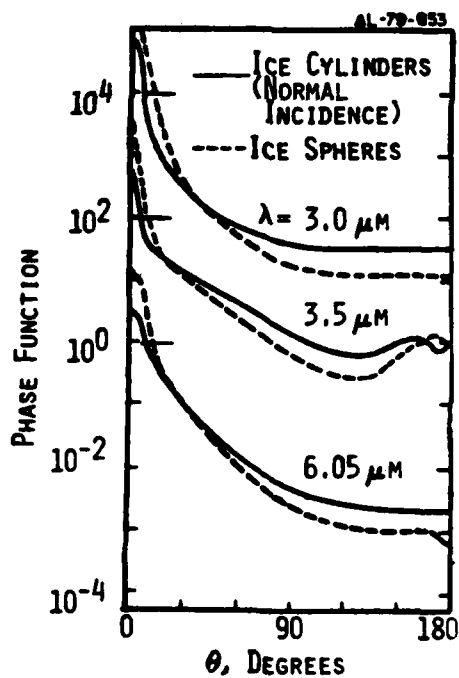


Figure 4. Scattering Phase Function for Uniformly Oriented Ice Spheres at Three Different Wavelengths. The Curves are Displaced for Clarity and the Horizontal Lines Through the Curves Correspond to the Value 1.0. From Ref. (18).

<sup>18</sup>Liou, Kuo-Nan, "Light Scattering by Ice Clouds in the Visible and Infrared: A Theoretical Study," J. Atmo. Sci., 29, 524 (1972).

Detailed Mie calculations for every particle size, wavelength, and scattering angle are time consuming and beyond the scope of an engineering type model. Therefore, a function which approximates the phase functions derived from Mie calculations is used in the model development. The most widely used and studied phase function is the Henyey-Greenstein (H-G) function, which was first introduced in 1941.<sup>(19)</sup>

$$P_{\text{H-G}}(\cos \theta_s) = \frac{(1 - g^2)}{(1 + g^2 - 2g \cos \theta_s)^{3/2}}, \quad (4)$$

where  $\cos \theta_s$  is the cosine of the scattering angle. The advantage of this scattering function over detailed results from Mie theory is that it provides a reasonable one-parameter fit to the detailed calculations for the angular distribution of light scattering by spherical droplets. The parameter is the asymmetry factor  $g$ , which is defined as the mean value of  $\mu_s$ , the cosine of the scattering angle. Figure 5 shows a comparison of the Henyey-Greenstein representation with Mie theory.<sup>(2)</sup> The H-G curve gives a reasonable overall description, although it does not have the small back scattering increase of the Mie calculation. The back scattering peak could be easily parameterized with a second H-G phase function. Figure 6, which is also taken from the work of Hansen,<sup>(3)</sup> shows a similar comparison for exact calculations of cloud directional radiance for two different optical depths and solar angles. In the present model, spectral variation in the phase function is introduced by varying the asymmetry parameter  $g$ , based on published Mie calculations.<sup>(16)</sup>

Molecular absorption by the atmospheric gases within clouds moderates the intensity of multiple scattering within the clouds for those spectral bands where the gases absorb strongly. In these spectral regions a photon

<sup>19</sup> Henyey, L.G. and Greenstein, J.L., "Diffuse Radiation in the Galaxy," Astrophys. J., 93, 70 (1941).

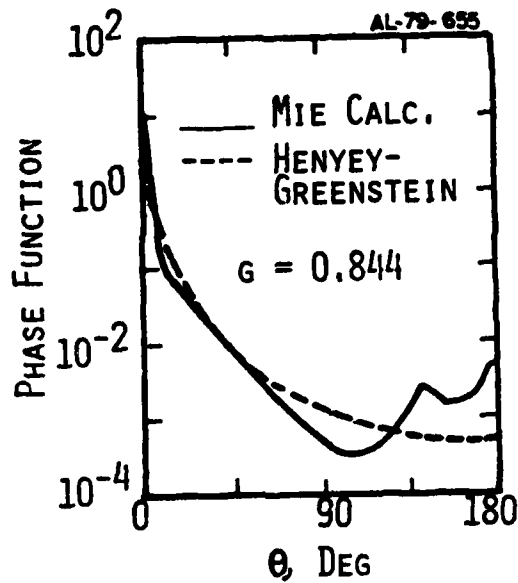


Figure 5. Comparison of the Angular Distribution of the Henyey-Greenstein Phase Function to Calculations from Mie Theory. From Ref. (3).

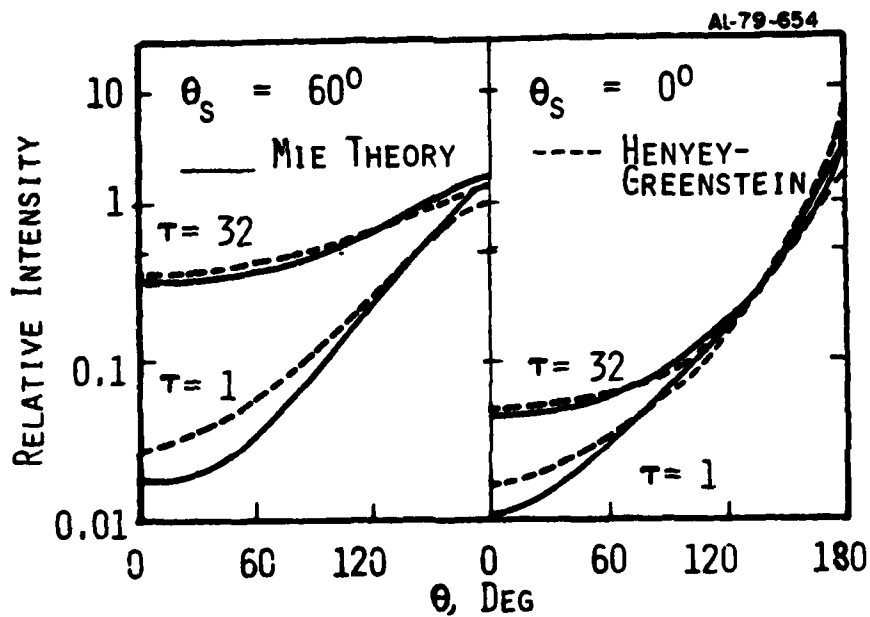


Figure 6. Comparison of the Angular Distribution at Two Optical Depths from A Cloud For Two Solar Azimuth Angles. An Exact Calculation with Mie Theory is Compared to One With the Henyey-Greenstein Phase Function. The Wavelength is  $0.7 \mu\text{m}$ . From Ref. (3).

will have little opportunity for more than one or two scattering events before being absorbed. The effect of molecular absorption is handled by modifying the single particle scattering albedo, which is defined as the ratio of the scattering to extinction cross sections. Under this assumption the albedo  $\omega$  is given by

$$\omega = \frac{\sigma_s}{\sigma_e + \kappa_v} \quad (4a)$$

where  $\sigma_s$  is the single particle volume scattering coefficient,  $\sigma_e$  is the particle extinction, and  $\kappa_v$  is the molecular volume absorption coefficient. Thus the effective single-particle scattering is reduced as the molecular absorption coefficient becomes larger.

### 2.2.2 Multiple Scattering

The multiple scattering term, which is the second one in the radiation transport equation, Eq. (1), describes the contribution of ambient radiation scattered into the observer's LOS. It is this term which makes Eq. (1) unsolvable in closed form. Highly accurate numerical solutions can be obtained using Monte Carlo calculational techniques. Such calculations, which follow the path of every photon, are not suitable for a quick, flexible model with its emphasis on describing the overall FOV scene with allowances for variations in the scene and viewing parameters. However, Monte Carlo calculations are extremely useful as a check on more approximate models.

The model which we selected approximates the multiple scattering integral by two terms.<sup>(13,18)</sup> These terms can be considered as the upwelling and downwelling radiance. The integral over  $\mu'$  or  $\cos \theta'$  in Eq. (1) is approximated by integrals over the upper and lower hemispheres, with the assumption of isotropic intensity in each hemisphere. Once this assumption is made, Eq. (1) becomes a set of two coupled differential equations for the upward and downward radiance.

The two-stream modeling approach has been used extensively in the cloud literature, especially in Refs. (7) to (10), and variations in detailed approaches are reviewed in Ref. (20). These studies are best summarized by saying that the two-stream model gives good results for the total upwelling radiance and adequate results for directional scattering. Although detailed comparisons with exact scattering models have not been made for arbitrary scattering geometries, we have found that the two-stream approach predicts directional results which are in good agreement with an exact Monte Carlo model,<sup>(21)</sup> for the case of zenith sun.

### 2.3 Two-Stream Model

The formulation of the present cloud model is based on several assumptions. A cloud of arbitrary and varying optical thickness is modeled by a plane parallel atmosphere in which the single scattering albedo ( $\omega_v$ ) is independent of depth. Local thermodynamic equilibrium between particles and atmospheric gases is assumed, with a uniform temperature throughout the cloud. With these assumptions, the equation of radiative transfer (with total extinction optical depth  $\tau$  as the independent variable) is

$$\mu \frac{dI_v}{d\tau} = I_v - \frac{1}{4\pi} \int_{-1}^1 \int_0^{2\pi} P(\mu, \phi; \mu', \phi') I(\tau, \mu', \phi') d\phi' d\mu' - (1 - \omega_v) B_v(T) - \frac{F}{4} \exp(-\tau/\mu_0) P(\mu, \phi; -\mu_0, \phi_0) \quad (4)$$

<sup>20</sup> Meador, W.E., and Weaver, W.R., "Two-Stream Approximations to Radiative Transfer in Planetary Atmospheres: A Unified Description of Existing Methods and a New Improvement," J. Atmo. Sci. 37, 630 (1980).

<sup>21</sup> Bernstein, L.S., Duff, J.S., Stanton, A.C., and Robertson, D.C., in preparation.

This equation may be rewritten in terms of a source function  $J_\nu(\tau)$  as<sup>(12,13)</sup>

$$\mu \frac{dI_\nu}{d\tau} = I_\nu - J_\nu \quad (5)$$

Equation (5) may be solved formally for the emergent radiance at the top of the cloud. The formal solution is

$$I_\nu(\tau = 0, \mu) = I_\nu(\tau_1, \mu) e^{-\tau_1/\mu} + \int_0^{\tau_1} J_\nu(\tau, \mu) \frac{e^{-\tau/\mu}}{\mu} d\tau, \quad (6)$$

where  $\tau_1$  is the optical thickness of the cloud. Because the source function  $J_\nu$  includes the multiple scattering term which involves the unknown radiance, an approximate method is adopted for solving the radiative transfer equation. This method consists of two steps. In the first step, the two-stream approximation is made and the multiple scattering integral is represented by integrals over the upper and lower hemispheres. In the second step, the approximate multiple scattering solution obtained in the first step is combined with the thermal emission term and an exact representation of the single scattering term. These terms form the source function, which is used in the formal solution, Eq. (6).

The azimuthally averaged form of the radiative transfer equation is used in developing the approximation for multiple scattering. This form of the equation is

$$\mu \frac{dI}{d\tau} = I - \frac{\omega}{2} \int_{-1}^1 P(\mu, \mu') I(\mu') d\mu' - (1 - \omega)B - \frac{F\omega}{4} \exp(-\tau/\mu_0) P(\mu, -\mu_0) \quad (7)$$

$$\text{where } \frac{1}{2} \int_{-1}^1 P(\cos \theta) d(\cos \theta) = 1. \quad (8)$$

The two-stream approximation is made by assuming that the radiance is independent of zenith angle in each of the upper and lower hemispheres, i.e.,

$$\begin{aligned} I(\mu) &= I^+, \quad 0 \leq \mu \leq 1 \\ I(\mu) &= I^-, \quad -1 \leq \mu \leq 0. \end{aligned} \quad (9)$$

Equation (7) may then be integrated over the upper and lower hemispheres to form two coupled equations in  $I^+$  and  $I^-$ :

$$\begin{aligned} \frac{1}{2} \frac{dI^+}{d\tau} &= I^+ - \frac{\omega}{2} (I^+ + I^-) - \frac{\omega H}{2} (I^+ - I^-) - (1 - \omega)B \\ &\quad - \frac{F}{4} \exp(-\tau/\mu_0) \omega [1 - G(\mu_0)], \end{aligned} \quad (10)$$

$$\begin{aligned} -\frac{1}{2} \frac{dI^-}{d\tau} &= I^- - \frac{\omega}{2} (I^+ + I^-) + \frac{\omega H}{2} (I^+ - I^-) - (1 - \omega)B \\ &\quad - \frac{F}{4} \exp(-\tau/\mu_0) \omega [1 + G(\mu_0)], \end{aligned} \quad (11)$$

$$\text{where } G(\mu) = \int_0^1 P(\mu, \mu') d\mu' = 1, \quad (12)$$

$$H = \int_0^1 G(\mu) d\mu. \quad (13)$$

The quantities  $G(\mu)$  and  $H$ , which involve hemispherical integrals of the scattering phase function, have been evaluated for the Henyey-Greenstein function in Ref. (22).

The boundary conditions for the problem are given by continuity of the radiance at the cloud top ( $\tau = 0$ ) and cloud bottom ( $\tau = \tau_1$ ):

$$I^-(\tau = 0) = 0, \quad (14a)$$

$$I^+(\tau = \tau_1) = I_B(\mu). \quad (14b)$$

Equation (14a) states that the diffuse downward-directed radiance at the cloud top is zero. Equation (14b) equates the upward-directed diffuse radiance at the cloud bottom to  $I_B(\mu)$ , which represents the upwelling radiance from the ground (thermal emission and solar scatter) plus atmospheric emission along the path from the ground to the cloud.

Equations (10) and (11) with boundary conditions (14a) and (14b) are sufficient to solve for  $I^+$  and  $I^-$ , the initial approximations to the upward and downward diffuse radiance. The details of this solution are algebraically tedious and will not be given here. After this solution is obtained, the approximate source function is formed as

$$J_\nu(\tau) \cong \frac{\omega}{2} (I^+ + I^-) + \frac{\omega}{2} G(\mu)(I^+ - I^-) + (1 - \omega)B_\nu(T) \\ + \frac{F}{4} \omega \exp(-\tau/\mu_0) P_{H-G}(\mu, \phi; -\mu_0, \phi_0). \quad (15)$$

With an approximation to the source function now defined, the solution for the emergent radiance at the top of the cloud may be found from Eq. (6). This solution is given here for completeness:

<sup>22</sup> Wiscombe, W.J., and Grams, G.W., "The Backscattered Fraction in Two-Stream Approximations," J. Atmo. Sci. 33, 2440 (1976).

$$\begin{aligned}
I(\mu) = & \frac{r_1 \omega_\nu}{2\mu} [-f + G(\mu)] \frac{1 - e^{-\tau_1(\lambda + \frac{1}{\mu})}}{\lambda + \frac{1}{\mu}} \\
& + \frac{r_2 \omega_\nu}{2\mu} [f + G(\mu)] \frac{1 - e^{\tau_1(\lambda - \frac{1}{\mu})}}{\frac{1}{\mu} - \lambda} \\
& + \frac{\omega_\nu}{2\mu} [\gamma + \alpha G(\mu)] \frac{1 - e^{-\tau_1(\frac{1}{\mu} + \frac{1}{\mu_0})}}{\frac{1}{\mu} + \frac{1}{\mu_0}} \\
& + B_\nu(T) [1 - e^{-\tau_1/\mu}] + \frac{F\omega_\nu}{4} P_{HG} \frac{1 - e^{-\tau_1(\frac{1}{\mu} + \frac{1}{\mu_0})}}{\frac{1}{\mu_0} + \frac{1}{\mu}} \\
& + I_B e^{-\tau_1/\mu} .
\end{aligned} \tag{16}$$

In this equation,  $\mu$  is the cosine of the observer zenith angle,  $\mu_0$  is the cosine of the solar zenith angle,  $\tau_1$  is the total extinction optical thickness of the cloud in the vertical direction,  $\pi F$  is the solar irradiance at the top of the cloud,  $B_\nu(T)$  is the Planck function, and  $I_B$  is the upwelling radiance at the lower boundary of the cloud. Other terms in this equation are:

$$r_1 = \frac{e^{\lambda\tau_1}(1+f) [\gamma - \alpha + 2B] - (1-f) [2I_B - 2B - (\gamma + \alpha)e^{-\tau_1/\mu_0}]}{(1+f)^2 e^{\lambda\tau_1} - (1-f)^2 e^{-\lambda\tau_1}} \tag{17}$$

$$r_2 = \frac{-e^{-\lambda\tau_1}(1-f) [\gamma - \alpha + 2B] + (1+f) [2I_B - 2B - (\gamma + \alpha)e^{-\tau_1/\mu_0}]}{(1+f)^2 e^{\lambda\tau_1} - (1-f)^2 e^{-\lambda\tau_1}}, \quad (18)$$

$$\gamma = \frac{\frac{-F}{2} \omega}{1 - \mu_0^2 \lambda^2} \left( \frac{\mu_0}{\bar{\mu}} \right) \left[ \frac{\mu_0}{\bar{\mu}} (1 - \omega H) + G(\mu_0) \right], \quad (19)$$

$$\alpha = \frac{\frac{F}{2} \omega}{1 - \mu_0^2 \lambda^2} \left( \frac{\mu_0}{\bar{\mu}} \right) \left[ 1 + \frac{\mu_0}{\bar{\mu}} (1 - \omega) G(\mu_0) \right], \quad (20)$$

$$\lambda^2 = \frac{1}{\bar{\mu}^2} (1 - \omega)(1 - \omega H), \quad (21)$$

$$f = \frac{1 - \omega H}{\lambda \bar{\mu}}. \quad (22)$$

#### 2.4 Implementation of the Cloud Model

The cloud model is implemented as a modification to the AFGL atmospheric transmittance code LOWTRAN3B.<sup>(23)</sup> A cloud layer of arbitrary altitude and spatial thickness is defined in the LOWTRAN input atmospheric profile by specifying

<sup>23</sup>Selby, J.E.A., Shettle, E.P., and McClatchey, R.A., "Atmospheric Transmittance from 0.25 to 28.5  $\mu\text{m}$ : Supplement LOWTRAN3B," AFGL-TR-76-0258, Air Force Geophysics Laboratory, Hanscom AFB, MA 01731 (November 1976). ADA040701.

the aerosol number density, temperature, and water vapor concentration in the cloud. Standard model atmospheres or radiosonde data are used to specify the rest of the atmospheric profile. Aerosol extinction and absorption coefficients which pertain to liquid water droplets or ice particles are used instead of the properties corresponding to the standard LOWTRAN atmospheric aerosol models. These wavelength-dependent coefficients are taken from Mie theory calculations by Shettle,<sup>(16)</sup> as reported by Zachor, et al.<sup>(15)</sup> A log-normal particle size distribution,

$$\frac{dN(r)}{dr} = \frac{1}{\sqrt{2\pi}\sigma} \exp \left[ -\frac{(\log r - \log r_m)^2}{2\sigma^2} \right], \quad (23)$$

was assumed in Shettle's calculations, and results are available for both water and ice for a range of mean particle sizes. The modified LOWTRAN code combines these aerosol parameters with its molecular absorption band model to calculate the transmittance through the cloud layer.

A special subroutine is added to the code to calculate the cloud radiance, including cloud thermal emission, scattered solar radiation, and scattered or directly transmitted upwelling radiance from below the cloud. This calculation is an evaluation of Eq. (16) above. The calculation of cloud radiance from Eq. (16) requires values for the wavelength dependent quantities  $\omega_V$ ,  $g$ ,  $F$ ,  $\tau_1$ , and  $I_0$ . The single scattering albedo is calculated as

$$\omega_V = \frac{n_p \sigma_{scat}}{n_p \sigma_{ext} + n_g \sigma_g}, \quad (24)$$

where  $n_p \sigma_{scat}$  and  $n_p \sigma_{ext}$  are the volume particle scattering and extinction coefficients and  $n_g \sigma_g$  is the volume gas absorption coefficient. Molecular absorption effects included in the cloud model are therefore characterized

by the LOWTRAN transmittance model, i.e., band and continuum absorption by important atmospheric gases are considered, with a spectral resolution of  $20 \text{ cm}^{-1}$ . The anisotropy parameter,  $g$ , which characterizes the single scattering phase function, is specified as input to the model using the results of the Mie theory calculations by Shettle.<sup>(16)</sup> The solar flux  $\pi F$  incident at the cloud top is given by

$$\pi F(\nu) = H_0(\nu) \cdot \tau_{\nu}(\infty \rightarrow \text{cloud}) \quad , \quad (25)$$

where  $H_0(\nu)$  is the solar irradiance at the top of the atmosphere and  $\tau_{\nu}(\infty \rightarrow \text{cloud})$  is the atmospheric transmittance from the top of the atmosphere to the cloud top, calculated by LOWTRAN. The cloud optical thickness,  $\tau_1(\nu)$ , may be obtained from the LOWTRAN transmittance calculations and includes the effects of gaseous absorption, aerosol absorption, and aerosol scattering. The diffuse spectral radiance at the bottom of the cloud,  $I_0$ , is calculated by LOWTRAN with the addition of solar scatter, and is given by

$$I_0(\nu) = \left[ \epsilon_g B_{\nu}(T_g) + r_g H_0 \frac{\cos \theta_0}{\pi} \cdot \tau(\infty \rightarrow \text{ground}) \right] \cdot \tau(\text{ground} \rightarrow \text{cloud}) + \int_{\text{ground}}^{\text{cloud}} B_{\nu}(T) \frac{\partial \tau}{\partial z} dz \quad . \quad (26)$$

Equation (26) includes the effects of ground thermal emission, sunlight scattered from the ground, and emission from atmospheric gases beneath the cloud. The ground emissivity  $\epsilon_g(\nu)$  and reflectivity  $r_g(\nu)$  are input parameters in the model.

The apparent cloud signal at observer altitude is calculated as

$$I(\nu) = I_{\text{cloud}}(\nu) \cdot \tau(\text{cloud} \rightarrow \text{observer}) + \int_{\text{cloud}}^{\text{observer}} B_{\nu}(T) \frac{\partial \tau}{\partial z} dz . \quad (27)$$

In this expression,  $I_{\text{cloud}}(\nu)$  is the cloud source radiance calculated according to Eq. (16) as described above,  $\tau(\text{cloud} \rightarrow \text{observer})$  is the atmospheric transmittance between the cloud top and the observer, and the integral term is the emission from atmospheric gases between the cloud and the observer.

To summarize this section, the cloud model is combined with the LOWTRAN atmospheric transmission model to form a general atmospheric radiative transfer code which is applicable to the calculation of infrared background signals (including clouds) which could be detected by high altitude downward-looking sensors. The inputs to the model are background characteristics (surface altitude, temperature, emissivity, and reflectivity), cloud characteristics (altitude, thickness, temperature, water vapor concentration, particle type, particle number density, and mean particle size), observer altitude, and observer and solar angles (zenith and azimuth). Standard atmospheric models or radiosonde data may be used to define the atmospheric profiles of temperature, water vapor concentration, etc. The output from the model is the calculated spectral radiance ( $20 \text{ cm}^{-1}$  resolution) at the observer's position due to thermal emission from clouds and the earth surface, sunlight scattered by clouds and earth surface, and thermal emission from the atmosphere. Integrated signals may be calculated for specified bandpasses.

## 2.5 Other Cloud Modeling Work

Two previous cloud modeling efforts, which have directly addressed the prediction of directional radiances in spectral bandpasses of possible interest for surveillance applications, are a study by S.J. Young<sup>(24)</sup> at the Aerospace Corporation, and cloud modeling work at Honeywell by Zachor, Holzer, and Smith.<sup>(15)</sup> Young's work<sup>(24)</sup> reviews several approximate schemes for calculating scattered radiation from clouds and adopts a method which is an empirical modification of a single-scattering model. Comparisons with exact solutions are given. In the work of Zachor, et al.,<sup>(15)</sup> an approximate two-stream solution to the radiative transfer equation is developed, and the solution is compared with the cloud data obtained in the 2.5 - 6  $\mu\text{m}$  region by the AFGL KC135A Flying Laboratory. The model discussed in this report is similar to the model of Zachor, et al., with the important difference that molecular absorption by atmospheric gases is included in the model. In addition, the present model ensures that the proper amount of energy is scattered into the upper and lower hemispheres. Incorporating the present model in LOWTRAN permits an evaluation of atmospheric attenuation and background source effects on the apparent cloud signature. These effects are very important in calculating cloud radiance within molecular absorption bands and for predicting the effects of cloud altitude on apparent cloud signal.

---

<sup>24</sup> Young, S.J., "Scattering of Solar Radiation by Clouds," The Aerospace Corporation Report TR-0079 (4970-40) -1, December 1978.

### 3. COMPARISONS WITH CLOUD SPECTRAL DATA

In this section the cloud radiance model is compared to cloud IR signature data taken from two different aircraft viewing platforms. The observations were made in the downward looking mode from above a solid cirrus cloud deck in the 2.5-6.0  $\mu\text{m}$  spectral region. The measurement platforms were a U2 aircraft at 15 km altitude and a KC135A aircraft at 5-10 km. The IR signature in the shorter wavelength region is dominated by solar radiation singly and multiply scattered by the cloud deck. At longer wavelengths thermal emission from the cloud itself becomes increasingly important. The next subsection discusses comparisons of model calculations for data taken by Arthur D. Little Co. from a U2 aircraft,<sup>(25)</sup> and the second subsection compares model calculations to AFGL data taken from a KC135A aircraft.<sup>(26, 15)</sup> Both of these measurements have the same general viewing geometry, a schematic of which is shown in Fig. 7. The sun was near the horizon so these data are for small total scattering angles ( $\theta_s \sim 10-15^\circ$ , as defined in Eq. (4)). One data comparison is made with the incident solar direction and measurement direction at right angles so that  $\theta_s \approx 89^\circ$ .

#### 3.1 2.7 $\mu\text{m}$ H<sub>2</sub>O/CO<sub>2</sub> Band

Measurements were taken over a cumulus/cirrus cloud deck with its top at an altitude of 15.25 km.<sup>(25)</sup> The measurements were made from a U2 flying 300 m above the clouds. A spectroradiometer was used to take data in the

---

<sup>25</sup> Espinola, R.P., "Spectral and Spatial Properties of Cloud Backgrounds From 2.65 to 2.95 Microns," Report No. 70505F, Arthur D. Little, Inc., Cambridge, MA 02140 (1970).

<sup>26</sup> Sandford, B.P., Schummers, J.H., Rex, J.D., Shumsky, J., Huppi, R.J., and Sluder, R.B., "Aircraft Signatures in the Infrared 1.2 to 5.5 Micron Region. Volume I: Instrumentation," AFGL-TR-76-0133, Air Force Geophysics Laboratory, Hanscom AFB, MA 01731 (1976). ADB014088L.

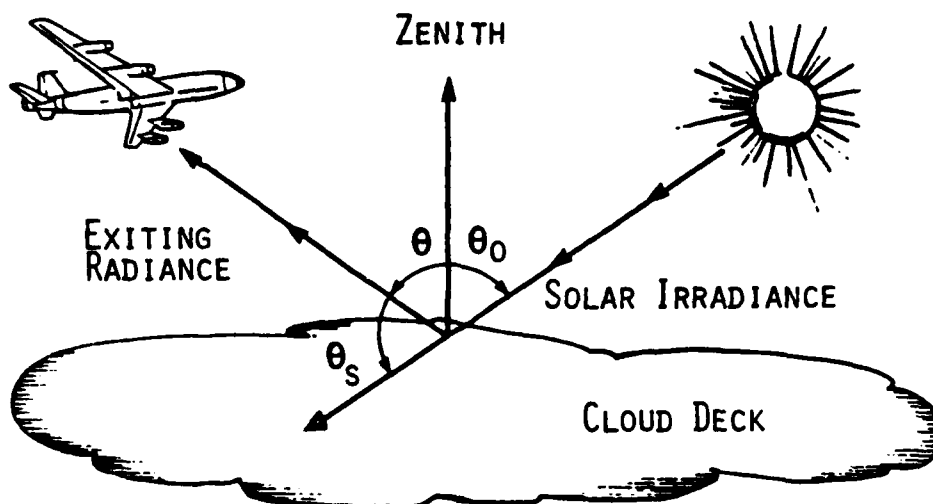


Figure 7. Schematic Showing the Measurement Geometry for Radiation From the Top of A Uniform Horizontal Cloud Deck. In This Example the Observing Aircraft is Looking Towards the Sun, so the Aspect Angle  $\phi$  Between the Incident Solar Direction and Exiting Radiation is Zero.

2.65-2.95  $\mu\text{m}$  region, with a spectral bandpass of 0.02  $\mu\text{m}$ . The uncertainty in this spectral region is 10% for each measurement with a minimum uncertainty of approximately  $10^{-6}$  watts/sr/cm<sup>2</sup>/ $\mu\text{m}$ . At the time of measurement the sun was near the horizon with a zenith angle of  $88^\circ$ . The U2 aircraft was looking down from an altitude of 15.5 km or approximately 1000 ft above the cloud deck with an observer zenith angle of  $80^\circ$ . The aircraft was looking almost directly towards the sun with a relative polar angle of  $1^\circ$ . The scattering angle between the incident and outgoing radiation is  $12^\circ$ .

Figure 8 shows a comparison of data taken by ADL with calculations using the Aerodyne cloud scattering model. The key features in the data are the strong  $\text{CO}_2$  absorption bands at 2.69 and 2.77  $\mu\text{m}$ , which lead to high altitude absorption of the incident solar energy. Although there is no information on the particle type and size distribution, ice crystals are certainly dominant because of the high altitude. The calculations assumed a mean

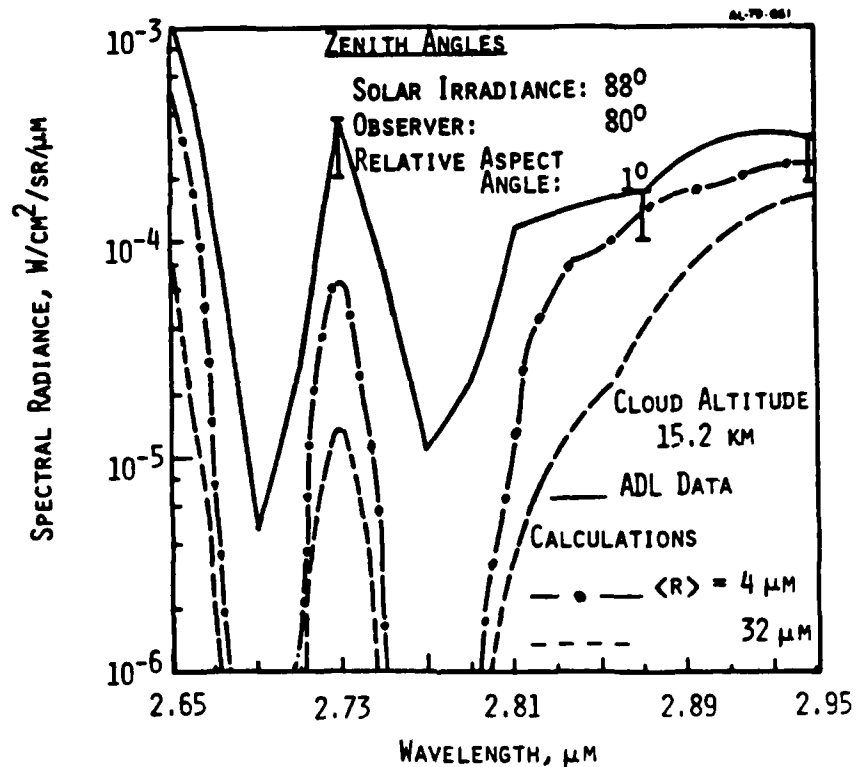


Figure 8. Comparison of Model Calculations to Arthur D. Little Data For Top Viewing of A Cloud in the 2.7  $\mu\text{m}$  Band. Two Calculations with Mean Particle Radii of 4 and 32  $\mu\text{m}$  are shown.

size of 32  $\mu\text{m}$  which is consistent with Liou's cylindrical crystal model<sup>(18)</sup> and with Hansen and Pollack.<sup>(2)</sup> The calculations capture the important spectral features of the data, i.e.,  $\text{CO}_2$  absorption and light scattering by the clouds, although they are consistently a factor of 3-10 below the data. The data vary by a factor of two, with Fig. 8 being the highest measured values.<sup>(25)</sup> The scattering angle of  $12^\circ$  is within the scattering peak, and the results are extremely sensitive to assumptions about the single-scatter phase function and details of the multiple scattering model.

As discussed in Section 2, the Henyey-Greenstein function gives good overall predictions for the intensities; however, it can be off by as much as a factor of 2 or more in its detailed angular dependence in the forward scattering peak. Uncertainties in the phase function for near-forward scattering are discussed below in subsection 3.2. Direct multiple scattering contributions (second and third scatterings) in the forward peak region will lead to increased radiation. The model in its present formulation includes multiple scattering in a diffusion approximation and direct single scattering. The calculations presented here are based on the log normal distributions and Mie theory calculations for the total scattering cross section.<sup>(16)</sup> Other calculations with different particle size distributions (Dermendjian Model,<sup>(17)</sup> with a mean radius of 4  $\mu\text{m}$ ) predict that the shorter wavelength contributions are enhanced by 10-30%. The comparisons of phase functions discussed below show that a factor of four variation in the detailed angular dependence can occur in the forward scattering peak.

### 3.2 Comparisons with AFGL Data

Interferometric measurements (1  $\text{cm}^{-1}$  resolution) of cloud spectral signatures were taken as part of the AFGL Aircraft Measurement Program.<sup>(26)</sup> The data discussed here pertain to a thick uniform cloud deck at an altitude of 9.3 km. The solar zenith angle was 82°. The measurements were taken from an altitude 0.7 km above the cloud, with an observer zenith angle of 87.5°. The relative azimuth angles (measured from the direction of forward scattering) are 0° (scattering angle  $\approx 10^\circ$ ) and 90° (scattering angle  $\approx 90^\circ$ ). Local radiosonde data were used to characterize the atmospheric conditions.

Comparisons of cloud model calculations with the AFGL spectral data are shown in Figs. 9 and 10. The cloud was assumed to consist of ice particles with a mean diameter of 32  $\mu\text{m}$ . The agreement between the model and data is good at the longer wavelengths, where the cloud thermal emission dominates solar scattering effects. The strong atmospheric absorption by  $\text{CO}_2$  in the 2200 - 2400  $\text{cm}^{-1}$  region is evident in both figures. At shorter wavelengths where the

scattered solar radiation is most important, the cloud model overpredicts the measured signal by a factor of 2 - 4 for the case of near-forward scattering (Fig. 9). In Fig. 10, the measured and predicted cloud signals at shorter wavelengths are lower by an order of magnitude than the forward scattering case, because the scattering angle is  $-90^\circ$ . The model and the data are in good agreement for this non-forward scattering case. Calculations performed by Zachor, et al.<sup>(15)</sup> are also shown in Figs. 9 and 10. The Zachor model is similar to the present model, with the exception that the present model accounts for molecular absorption between scattering events within the cloud. This feature is evident in Fig. 9, where water vapor absorption from  $3100 - 3500 \text{ cm}^{-1}$  leads to reduced solar scattering in the predictions of the present model.

For the case of near-forward scattering, the solar scattering contribution to the cloud signal is dominated by single scattering. In the single scattering limit the solution to the radiative transfer equation (optically thick cloud) reduces to the result,

$$I(\mu, \phi) = \frac{F\omega_v}{4} \frac{\mu_0}{\mu + \mu_0} P_{\text{H-G}}(\cos \theta_s) \quad (28)$$

The cloud radiance in this limit is thus directly proportional to the single scattering phase function. In the forward scattering peak, the phase function is sensitive to several detailed assumptions in the model (for example, the mean particle size or, in the case of ice crystals, the particle shape). The uncertainties in these assumptions give rise to an overall uncertainty in the model predictions, which represents an inherent limit in the accuracy of idealized models in predicting real cloud properties.

A range of values for the single scattering phase function  $P[\cos(10^\circ)]$  appropriate to the description of scattering by ice particles is given in Table 1. The table shows a comparison of the phase function from Mie theory

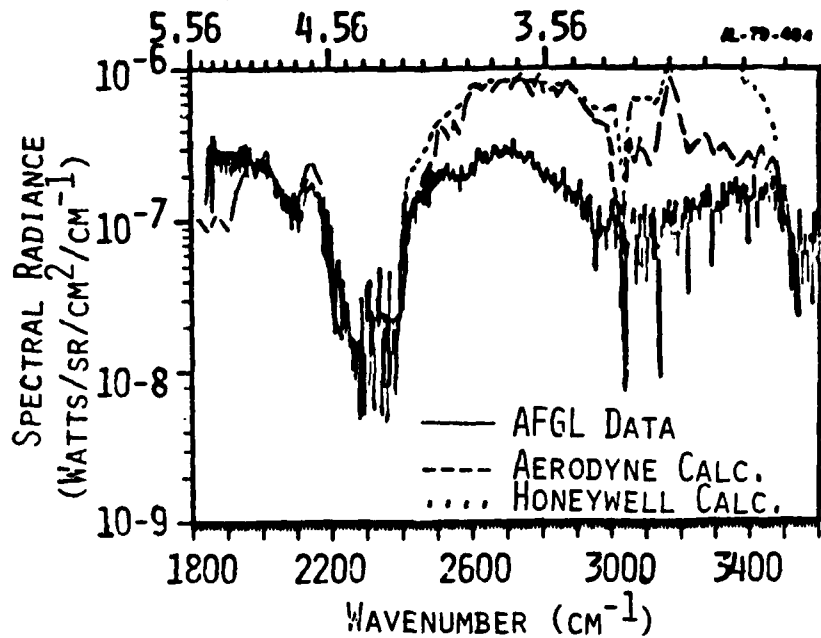


Figure 9. Comparison of Aerodyne and Honeywell Calculations to AFGL Data for Top Viewing of a Cloud Deck (Scattering Angle  $\cong 10^\circ$ ).

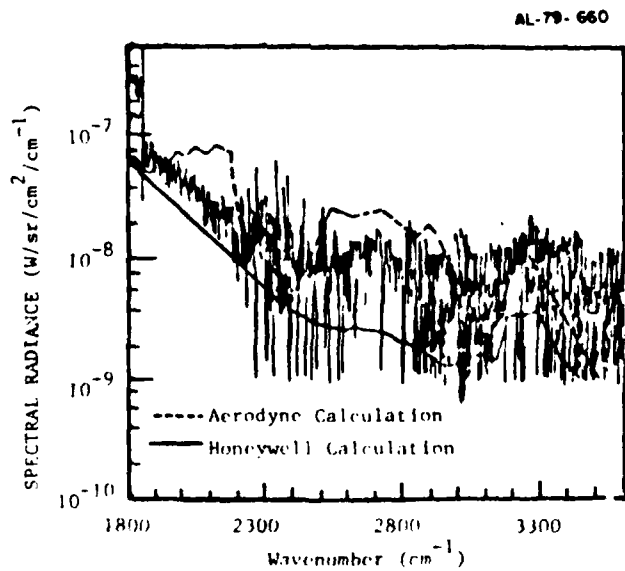


Figure 10. Comparison of AFGL Data to Honeywell and Aerodyne Calculation For Viewing the Same Cloud Deck as Fig. 9 (Scattering Angle  $\cong 90^\circ$ ).

Table 1. Comparison of Single Scatter Phase Functions in the Forward Scattering Peak (Scattering Angle =  $10^\circ$ )

$\lambda$ ( $\mu\text{m}$ )	P(cos $\theta$ )		Mie Theory <sup>(27)</sup>	
	Henyey-Greenstein Shettle <sup>(16)</sup>	Liou <sup>(27)</sup>	spheres	cylinders
2.5	1.09	4.52	-	-
3.0	1.94	2.10	-2	-8

calculations of Liou<sup>(27)</sup> for ice cylinders and ice sphere (30  $\mu\text{m}$  radius) with the Henyey-Greenstein function using asymmetry parameters calculated by Shettle<sup>(16)</sup> (32  $\mu\text{m}$  radius particles) and by Liou<sup>(27)</sup>. The comparison of the phase functions at  $\lambda = 3 \mu\text{m}$  indicates a factor of 4 variation. In the absence of detailed microphysical data on particle number density, size distribution, and particle shape, there is not a priori reason for preferring any of the phase functions in Table 1. A much broader base of data comparisons is required in order to identify the appropriate microphysical data for providing a consistent description of scattering from clouds.

The alternative phase functions listed in Table 1 would each result in a higher predicted cloud signal for the case presented in Fig. 9 than the present model predictions, which are based on the Henyey-Greenstein function using the Shettle<sup>(16)</sup> asymmetry parameters. This trend would result in poorer agreement with the data presented in Fig. 9. On the other hand, the difference in the ice cylinder and sphere phase functions at  $\lambda = 3.9 \mu\text{m}$  accounts for the difference between data and calculations for the high altitude clouds of Fig. 8. Other effects which are not considered in the model may be important, however. For example, surface "roughness" at the cloud top (which is assumed smooth in the idealized model) could result in a reduced single scattering contribution from the top layers of the cloud for the grazing geometry

<sup>27</sup>Liou, K.N., "Transfer of Solar Irradiance through Cirrus Cloud Layers," J. Geophys. Res., 78, 1409 (1973).

applicable to Fig. 9. As indicated in Fig. 11, surface roughness would result in attenuation of much of the forward scattered radiation, resulting in a significantly smaller cloud signal. A detailed consideration of these effects was outside the scope of the present study. For purposes of the present work, the two-stream cloud model shows good qualitative agreement with data in the spectral dependence of cloud signals. For near forward scattering geometries, however, quantitative agreement is sensitive to the detailed cloud microphysics and local scattering geometry.

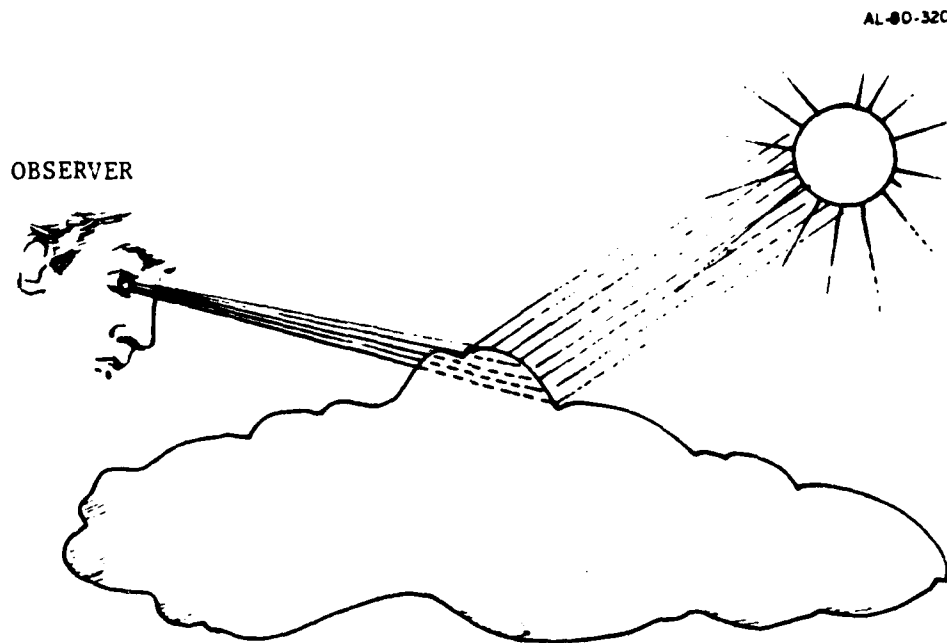


Figure 11. Attenuation of Singly Scattered Radiation by Cloud Surface Roughness.

## 4. COMPARISON OF MODEL PREDICTIONS WITH BAMM DATA

In this section, the Aerodyne cloud and background radiance model discussed in the previous sections is applied to the analysis of field data taken in the BAMM program.<sup>(28)</sup> These data consist of radiometer measurements in the 2.7-3.1  $\mu\text{m}$  region from the BAMM test flight of September 28, 1978 at Holloman Air Force Base, New Mexico. Model predictions are compared with BAMM measurements for several scene types, including a downward-looking stare scene through a clear atmosphere, an elevation scan over varied background including a feature which may be thin high-altitude cirrus, and an azimuthal scan over a background scene which includes broken fair weather cumulus clouds at lower altitudes.

### 4.1 Mountain Terrain Background (Clear Air)

The clear-air comparisons of calculated and measured radiance levels are made for a staring scene identified in the BAMM Data Report<sup>(28)</sup> as Scene Ic and Scene Id. This scene is a downward-looking stare (observer nadir angle = 1.8 - 3.1 $^{\circ}$ ) at the Sacramento Mountains. The background consists of forested, hilly terrain with the elevation varying between 7000' and 8500' (above sea level), as determined from U.S. Geological Survey topographic maps. For the three-minute stare sequences, the radiometer data show very little temporal or spatial variation, and the typical scene radiance values are 0.6  $\mu\text{W}/\text{cm}^2/\text{sr}/\text{band}$  for Filter 1 (wideband filter) and 0.1  $\mu\text{W}/\text{cm}^2/\text{sr}/\text{band}$  for Filter 2 (narrow band filter).<sup>(28)</sup>

The Aerodyne background radiance/cloud model was used to calculate expected levels of background radiance at the balloon altitude for Scene Ic

<sup>28</sup> Murphy, R.E., Cook, F.H., Grossbard, N.G., Grieder, W.F., and Yap, B.K., "Balloon Altitude Mosaic Measurements (BAMM) Data Report II," Air Force Geophysics Laboratory, Hanscom AFB, MA 01731 (1979).

and Scene Id. A baseline calculation using the "Holloman" radiosonde data (28 September 1978, 0630 MST) was performed. Further calculations were made to test the sensitivity of the calculations to atmospheric temperature and humidity profiles. The in-band radiances for BMM Filters 1 and 2 were determined for each case by integrating the calculated spectral radiance over the filter bandpasses, including the transmission functions of the filters. The input parameters for these calculations are given in Table 2. A uniform surface emissivity of 0.9 and reflectivity of 0.1 were assumed for the calculations. A high emissivity for botanical materials is expected due to their high cellulose and water contents.<sup>(29)</sup>

Table 2. Baseline Input Parameters for Background Radiance Calculations (Scene Ic and Scene Id)

Observer altitude	98,000 ft. (29.9 km)
Background altitude	7,000 ft. (2.13 km)
Observer Angle (zenith)	2.8°
Solar angle (zenith)	48.3°
Background emissivity	0.9 } (assumed constant
Background reflectivity	0.1 } with wavelength)
Background temperature	13°C
(Holloman radiosonde data)	

The results of the baseline calculation are given in Table 3. The calculated in-band radiances are shown in the table, along with measured in-band radiances from Scene I. The contributions of the various radiance components (ground thermal emission, ground solar scatter, and atmospheric thermal emission) to the total calculated values are also given in the table.

<sup>29</sup>Wolfe, W.L., and Zissis, G.J., Editors, The Infrared Handbook, (Office of Naval Research, Department of the Navy, Washington, DC, 1978).

Table 3. Baseline Radiance Calculation for Scene 1

In-Band Radiance, $W/cm^2/sr$					
Filter	Data	Calculations			
		Total	Thermal	Solar Scatter	Atmospheric
1	$6 \times 10^{-7}$	$3.86 \times 10^{-7}$	$5.18 \times 10^{-8}$	$2.42 \times 10^{-7}$	$9.22 \times 10^{-8}$
2	$1 \times 10^{-7}$	$0.70 \times 10^{-7}$	$0.76 \times 10^{-8}$	$0.38 \times 10^{-7}$	$2.44 \times 10^{-8}$

The sensitivity of the calculations to changes in the atmospheric temperature and humidity profiles is indicated by the results given in Table 4. The calculated in-band radiances are shown in this table for various atmospheric profiles, otherwise using the baseline input of Table 2. Looking at the ratio of calculated Filter 1 and Filter 2 band radiances in Table 4, we see that the ratio of the two bands is fairly insensitive to the atmospheric profile. Reasonably close agreement is obtained among the calculations made with the two sets of radiosonde data and the midlatitude summer model. The "Jallen" radiosonde data correspond to an ascension of time of 1330 MST on Sept. 28, whereas the "Holloman" ascension time was 0630 MST. The atmospheric profile for the Jallen (early afternoon) data is warmer and drier, resulting in reduced atmospheric absorption. This effect causes significant increases in reflected solar energy as measured at the observer altitude. The proportion of the total radiance which is due to reflected sunshine also increases due to the double transit of this radiation through the atmosphere. The fractions of the total radiance which are due to reflected solar radiation are given in Table 5 for the two atmospheric profiles.

Table 4. Calculated In-Band Radiance for Several Atmospheric Profiles

Atmospheric Model	Radiance, W/cm <sup>2</sup> /sr		N <sub>1</sub> /N <sub>2</sub>
	Filter 1	Filter 2	
Holloman Radiosonde	0.39 x 10 <sup>-6</sup>	0.70 x 10 <sup>-7</sup>	5.57
Jallen Radiosonde	0.52 x 10 <sup>-6</sup>	0.99 x 10 <sup>-7</sup>	5.26
Midlatitude Summer	0.48 x 10 <sup>-6</sup>	0.84 x 10 <sup>-7</sup>	5.74
1962 U.S. Standard	0.89 x 10 <sup>-6</sup>	1.8 x 10 <sup>-7</sup>	4.83
Observed	0.6 x 10 <sup>-6</sup>	1.0 x 10 <sup>-7</sup>	6.0

Table 5. Fraction of Calculated In-Band Radiance Due to Reflected Solar Radiation

Atmospheric Model	Reflected Solar Energy (Fraction of Total Radiance)	
	Filter 1	Filter 2
Holloman Radiosonde	0.62	0.54
Jallen Radiosonde	0.69	0.64

These calculations indicate that the modified LOWTRAN atmospheric transmission and background radiance model predicts levels of background radiance for this scene which are in good agreement with the BMM radiometer measurements. The predicted signal ratios between the two filters are consistent with the data. The absolute predicted radiance levels can be shifted somewhat, depending on the choice of background emissive and reflective properties. In these calculations, approximately 50-70% of the total background radiance is due to reflected sunlight. This fraction is highly dependent on the background elevation assumed in the calculations. For lower background elevations the atmospheric transmission decreases significantly,

primarily because of enhanced absorption by water vapor, and the fractional contribution of reflected sunlight to the total background radiance would be smaller. The model calculations discussed in the next subsection illustrate this effect.

#### 4.2 Elevation Scan: Desert/Mountain Background With Possible Cirrus Cloud

The first portion of the Scene I data (Scene Ia and Scene Ib) discussed in the BMM report<sup>(28)</sup> consists of an elevation scan, beginning at a maximum nadir angle of approximately  $69^\circ$  and scanning down to a minimum angle of approximately  $1.8^\circ$  (downward viewing). A radiometer (wideband filter) radiance-time plot for this scene is shown in Fig. 12.

The plots of absolute radiance versus time for the Scene I elevation scan (Scene Ia and Scene Ib) show several characteristic features. A general feature is the increase in average signal level as the elevation angle decreases. The mean signal level at maximum nadir angle ( $69.47^\circ$ ) is approximately 55% of its value at the minimum nadir angle. The increase in signal with decreasing nadir angle is mainly due to the increase in atmospheric transmittance for a shorter path from the ground to the balloon. Calculated atmospheric spectral transmittance for observer nadir angles of  $0^\circ$  and  $60^\circ$  are shown in Fig. 13. (A background elevation of 4100 ft is used in the calculations.) These LOWTRAN calculations, which include only atmospheric and surface thermal emission, show that the expected signal level at a nadir angle of  $69^\circ$  is approximately 75% of its value for downward-looking. The measured signal also includes a solar scattering component. This component becomes more strongly attenuated at the high nadir angles because the solar radiation which is reflected makes a double transit through the atmosphere. If diffuse solar scattering with a terrain reflectance of 0.1 is assumed, the LOWTRAN model predicts a variation in absolute radiance level which closely matches the measured dependence on nadir angle. This prediction is the dotted curve labeled "Aerodyne calculations" in Fig. 12. The fractional contribution of the solar scatter component increases from approximately 20%

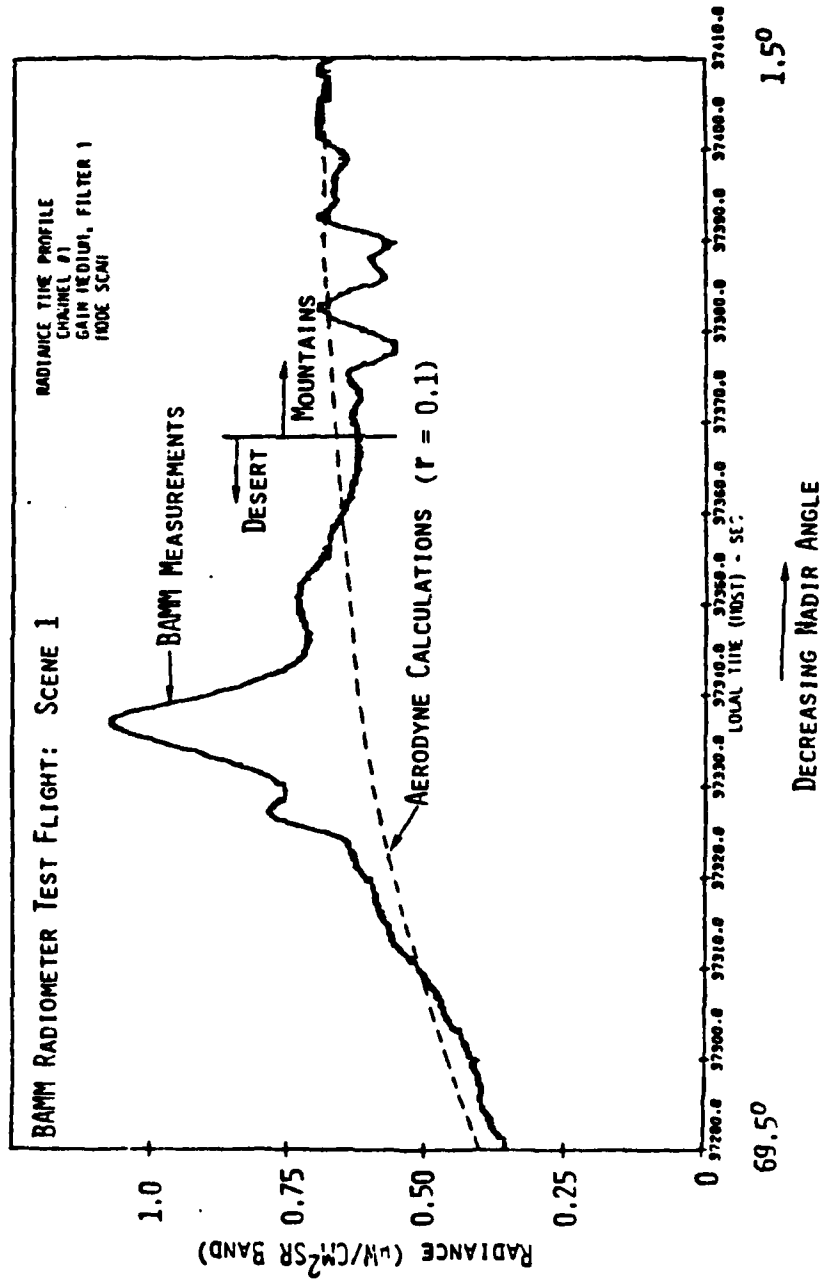
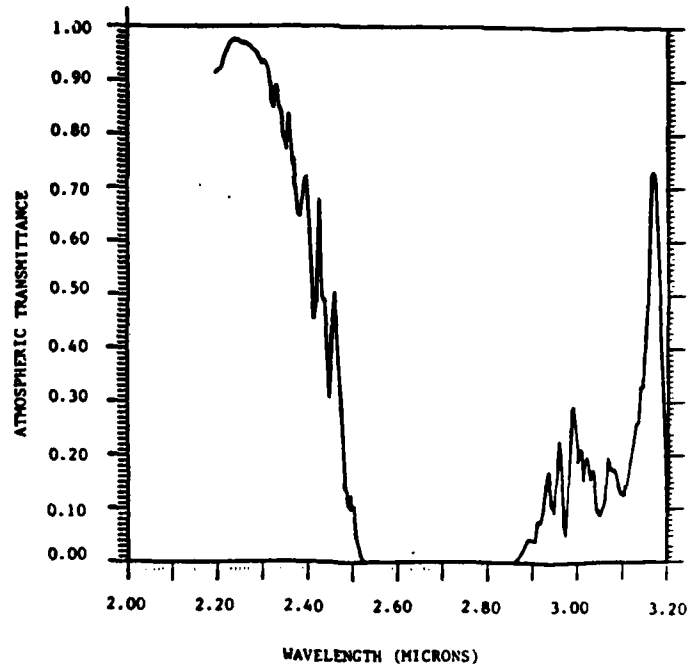
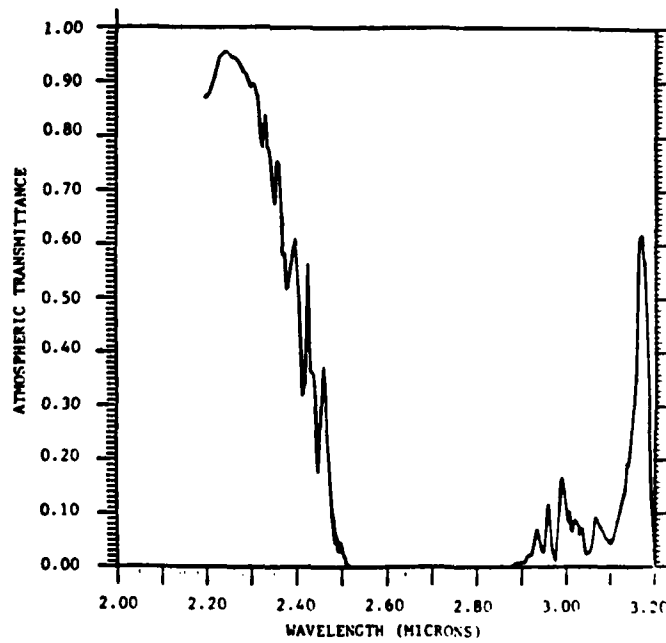


Figure 12. Comparison of Background Radiance Calculations With Bamm Radiometer Measurements for Scene Ia and Ib(24)



a) observer nadir angle = 0°



b) observer nadir angle = 60°

Figure 13. Calculated Atmospheric Transmittance for Two Observer Nadir Angles

at  $70^\circ$  to 37% at  $0^\circ$ . This fractional contribution is less than the scattering contributions discussed in the previous comparison (stare scene) because the earth background was at a lower elevation.

In addition to the overall increase in signal level which is due to the increasing atmospheric transmittance, two other features of the radiance-time plots for Scene Ia and Scene Ib are noteworthy. The first of these is the large increase in signal which occurs in Scene Ia at approximately 37330 sec (10:22:10). The signal in all channels increases by nearly a factor of two. This signal increase is correlated with a blurring of the scene in the television pictures. This blur, which does not totally obscure the terrain background, has not been positively identified. A likely explanation is that it is a thin cirrus cloud, however. This possibility is examined in more detail below. In the latter part of the elevation scan (Scene Ib), the signal in all channels shows variations which are correlated with spatial variations in the background. The background scene in this portion of the scan is the Sacramento Mountains with sunlit peaks and shadowed regions where the solar scatter contribution to the signal is reduced. The measured signal level is modulated by scanning over this spatially structured terrain.

The peak in the infrared signal in Scene Ia, which is correlated with a blur in the television pictures, suggests the possibility of a thin high altitude cloud. Such a cloud can transmit much of the upwelling radiance from the earth surface and the lower part of the atmosphere in addition to reflecting solar radiation. In particular, radiation in the  $2.7 \mu\text{m}$  water vapor bands which is scattered by high altitude clouds can lead to an enhanced background signal because the cloud is above most of the atmospheric water vapor attenuation. The two-stream cloud radiance model developed in Section 2 has been used to illustrate these effects and to examine the possibility that the signal deriving from the "blur" could be caused by a cirrus cloud at high altitudes. The results of these calculations are summarized in Table 6, where the calculated in-band radiance (BAMM Filter 1) for a background

Table 6. Calculated In-Band Radiance (BAMM Filter 1) For a Background Scene Including An Ice Cloud at 50,000 ft Altitude.

CLOUD THICKNESS (km)	TRANSMITTANCE (at = 3.2 $\mu\text{m}$ )	SCENE RADIANCE ( $\mu\text{W}/\text{cm}^2/\text{sr}$ )
0	1.0	0.6
0.1	0.97	1.1
0.2	0.95	1.4
1.0	0.82	3.6
Opaque Cloud	0.	14.

including a cloud at 50,000 ft altitude is shown for a range of cloud thicknesses. A particle concentration of  $0.01 \text{ cm}^{-3}$  was assumed for the calculations. Scattering and absorption properties for a distribution of ice particles with a mean particle radius of  $32 \mu\text{m}$  were used in the calculations.

The results in Table 6 demonstrate that scattering of sunlight from thin high-altitude clouds can result in significantly enhanced background signals, when the scattering effects are not blurred by atmospheric attenuation. The calculated band radiance for BAMM Filter 1 for a cloud with a transmittance of 0.95 at  $3.2 \mu\text{m}$  (0.2 km thickness) is more than twice the clear-air signal. The particle concentration of  $0.01 \text{ cm}^{-3}$  is consistent with or even smaller than typical particle concentrations in cirrus clouds.<sup>(8)</sup> The predicted signal enhancement for such a cloud is consistent with the observed enhancement evident in the radiometer data of Fig. 12.

The cloud altitude has a strong effect on possible background signal enhancement due to solar scattering. The altitude effect is illustrated in Fig. 14, which shows a comparison of calculated cloud radiance with the clear-air background radiance for two cloud altitudes. At high altitudes

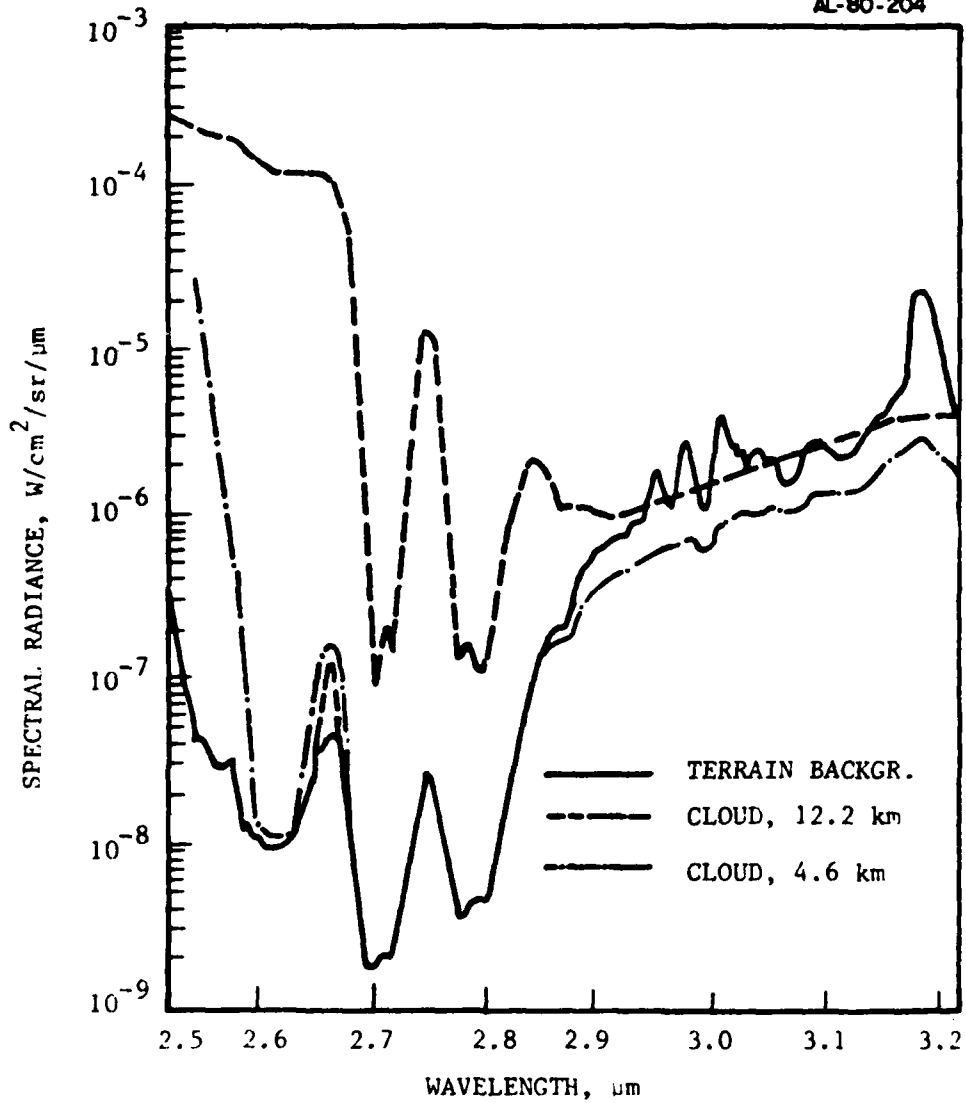


Figure 14. Comparison of Apparent Cloud Spectral Radiance (at observer altitude) and Clear-Air Background Radiance for two cloud altitudes.

(12.2 km), the cloud is above most of the atmospheric water vapor attenuation and the spectral radiance in the 2.5-2.8  $\mu\text{m}$  region is greatly enhanced by the presence of the cloud. Atmospheric attenuation by  $\text{CO}_2$  is evident in the calculated cloud spectral radiance. At lower altitudes (4.57 km), the cloud signal is strongly attenuated below 2.85  $\mu\text{m}$  by atmospheric  $\text{H}_2\text{O}$ . Beyond 2.85  $\mu\text{m}$ , the cloud signal may be either larger or smaller than the clear-air background signal, depending on the efficiency of the directional scattering of the cloud compared with diffuse scattering from the terrain background.

The BAMM television pictures offer no indication of the altitude of the "blur" which is evident in Scene Ia. As indicated in the discussion above, the infrared data for the scene are consistent with model predictions for an optically thin cloud at high altitudes. The cloud model was also used to simulate ground fog for the conditions of Scene Ia, by locating the model "cloud" as a layer just above ground elevation. For this case, the model calculations show that the fog inhibits transmission at wavelengths where molecular attenuation is not important, and the layer scatters sunlight less efficiently than the terrain background. Strong  $\text{H}_2\text{O}$  and  $\text{CO}_2$  attenuation prevents any significant contribution to the total signal below 2.85  $\mu\text{m}$ . The net effect is that the predicted radiance from the background with ground fog is reduced compared to the clear-air terrain background, with a maximum signal reduction of 25% for optically thick fog.

The model predictions discussed in this section show that high altitude clouds can produce strong IR background radiance signals in the 2.7-3.2  $\mu\text{m}$  region, and that the signals may be significantly larger than the background radiance for clear-air conditions. The effect is significant even for an optically thin cloud. This effect has probably been observed in BAMM Scene Ia; however the television pictures do not provide conclusive proof.

#### 4.3 Cumulus Clouds (Low Altitude)

The data from the BMM Holloman radiometer test flight show significant background radiance variations in Scene II, which is an azimuthal scan over a mountain background, with broken cumulus clouds.<sup>(28)</sup> The significant background features are sunlit terrain, shadowed terrain (from cloud shadowing), and cumulus clouds which are optically thick in the visible. The individual clouds are typically of a size such that they fill most of the field of view of one radiometer pixel. A radiance time profile for BMM Scene IIb (Fig. 29 reproduced from Ref. (28)) is shown in Fig. 15. The plot shows the measured radiance in one pixel for the three-minute scan, using Filter 1 (the wideband filter). By comparison of the data for all of the detector elements, the maximum measured radiance for the scan is approximately  $1.0 \mu\text{W}/\text{cm}^2/\text{sr}/\text{band}$ , with minimum radiance levels of approximately  $0.45 \mu\text{W}/\text{cm}^2/\text{sr}/\text{band}$ . A similar scan in Scene IIa with Filter 2 (narrow filter) resulted in measured radiance variations from approximately  $0.088 \mu\text{W}/\text{cm}^2/\text{sr}/\text{band}$  to maximum values of approximately  $0.16 \mu\text{W}/\text{cm}^2/\text{sr}/\text{band}$ . Comparison of the radiance time profiles with the television pictures indicates that the largest signals correspond to terrain backgrounds, intermediate signal levels correspond to clouds or mixed cloud-terrain backgrounds, and the lowest signal levels correspond to cloud shadows.

The two-stream cloud scattering model was used to calculate the expected radiance levels for clouds, cloud shadows, and sunlit terrain for the conditions of the Scene II azimuth scans. The background elevation was determined from USGS topographic maps, and cloud heights were estimated from the television pictures (based on the relative cloud and cloud shadow positions). The cloud calculations were carried out for the range of relative observer and solar azimuth angles corresponding to the measurement scan, however the results were insensitive to azimuth angle. The input conditions for the calculations are summarized in Table 7.

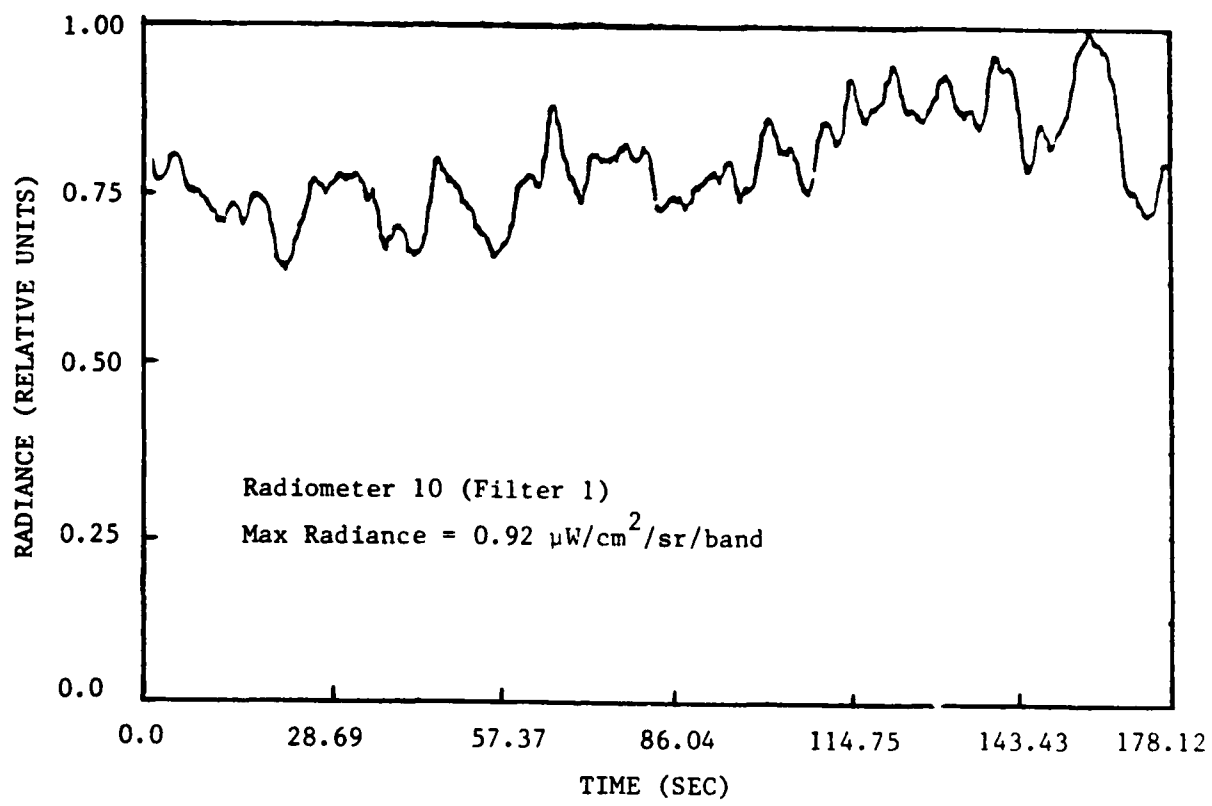


Figure 15. Radiance-Time Profile<sup>(24)</sup> for An Azimuthal Scan Over Cumulus Clouds

Table 7. Input Parameters for Low Altitude Cumulus  
Cloud Calculations (BAMM Scene II)

Terrain Background:	
Elevation	2.59 km
Temperature	20°C
Emissivity	0.90
Reflectivity	0.10
	} constant with wavelength
Atmospheric Profile	"Holloman" radiosonde
Cloud Background:	
Cloud Top Elevation	5.2 km
Cloud Thickness	1 km
Particle Density (Liquid H <sub>2</sub> O)	500 cm <sup>-3</sup>
Mean Particle Radius	4 μm
Observer Geometry:	
Elevation	30.2 km
Azimuth Angle	148.4-247.4°
Nadir Angle	24.4°
Solar Angles:	
Zenith	38.4°
Azimuth	153°

The calculated in-band radiance levels for the various background features are shown in Table 8. The expected radiance levels for cloud shadows are calculated by setting the solar scatter contribution to zero. The calculation thus includes only thermal radiation from the terrain background and from the atmosphere, with atmospheric attenuation. The predicted cloud shadow signal levels for both filters are in excellent agreement with the measured minimum signals during the scans.

Table 8. Calculated Radiance Levels (In-Band) for Background Features in BMM Azimuth Scans (Scene II)

Background	Radiance, $\mu\text{W}/\text{cm}^2/\text{sr}/\text{band}$	
	Filter 1 (Wide Filter)	Filter 2 (Narrow Filter)
Sunlit Terrain	2.0	0.39
Cumulus Clouds	0.64	0.13
Cloud Shadows	0.41	0.091

An apparent discrepancy between the measurements and the calculations arise in comparing the predicted radiance levels for sunlit terrain with the maximum measured signal. The predicted sunlit terrain radiance is a factor of 2 larger than the highest observed signals. In the case of terrain background, the solar scatter term is calculated by using a specified input reflectivity of 0.10. Variations of this quantity with wavelength, as well as a lower effective reflectivity due to surface roughness (terrain self-shadowing) may account for overprediction of the solar scatter. In addition, the background elevation assumed for the calculations (2.59 km or 8500') may be higher than the mean elevation during the scan, in which case the atmospheric attenuation is underestimated.

The qualitative trend of highest IR signals being correlated with sunlit terrain, intermediate signal levels being correlated with clouds, and minimum signal levels being due to cloud shadows is predicted by the cloud model. Exact

correlation of the television pictures with the infrared data is difficult, however, because the instantaneous field of view for any detector element typically includes some combination of cloud, cloud shadow, and sunlit background. The experimental differences between cloud radiance and sunlit terrain radiance for this scene are therefore difficult to assess.

Scene III from the BMM radiometer test flight<sup>(28)</sup> is a staring scene at a low altitude cumulus cloud. During the course of the stare sequence, the combination of cloud and platform drift causes the field-of-view for several of the detector elements to shift from mostly cloudy to mostly clear. Radiance-time profiles for this sequence show negligible long-term drift of the in-band radiance signal, suggesting little difference between cloud and terrain backgrounds in this instance. Figure 16 shows the measured radiance-time profile for Detector 7.<sup>(28)</sup> By comparison with the television pictures, the field-of-view for this detector changes from completely cloudy (visibly thick cloud) to almost completely clear (in the visible) over the course of the scan.

The experimental results from the radiometer test flight suggest that thick cumulus clouds at elevations around 4.6 km (15,000 ft) have little effect on the band radiance in the 2.7-3.1  $\mu\text{m}$  region. The cloud model calculations predict a more significant effect, however the strong radiance variations that were evident for the high altitude cirrus clouds are moderated by atmospheric attenuation at the lower altitudes. Further comparisons, especially emphasizing the spectral radiance from interferometer data, are required to validate the cloud model for low altitude clouds.

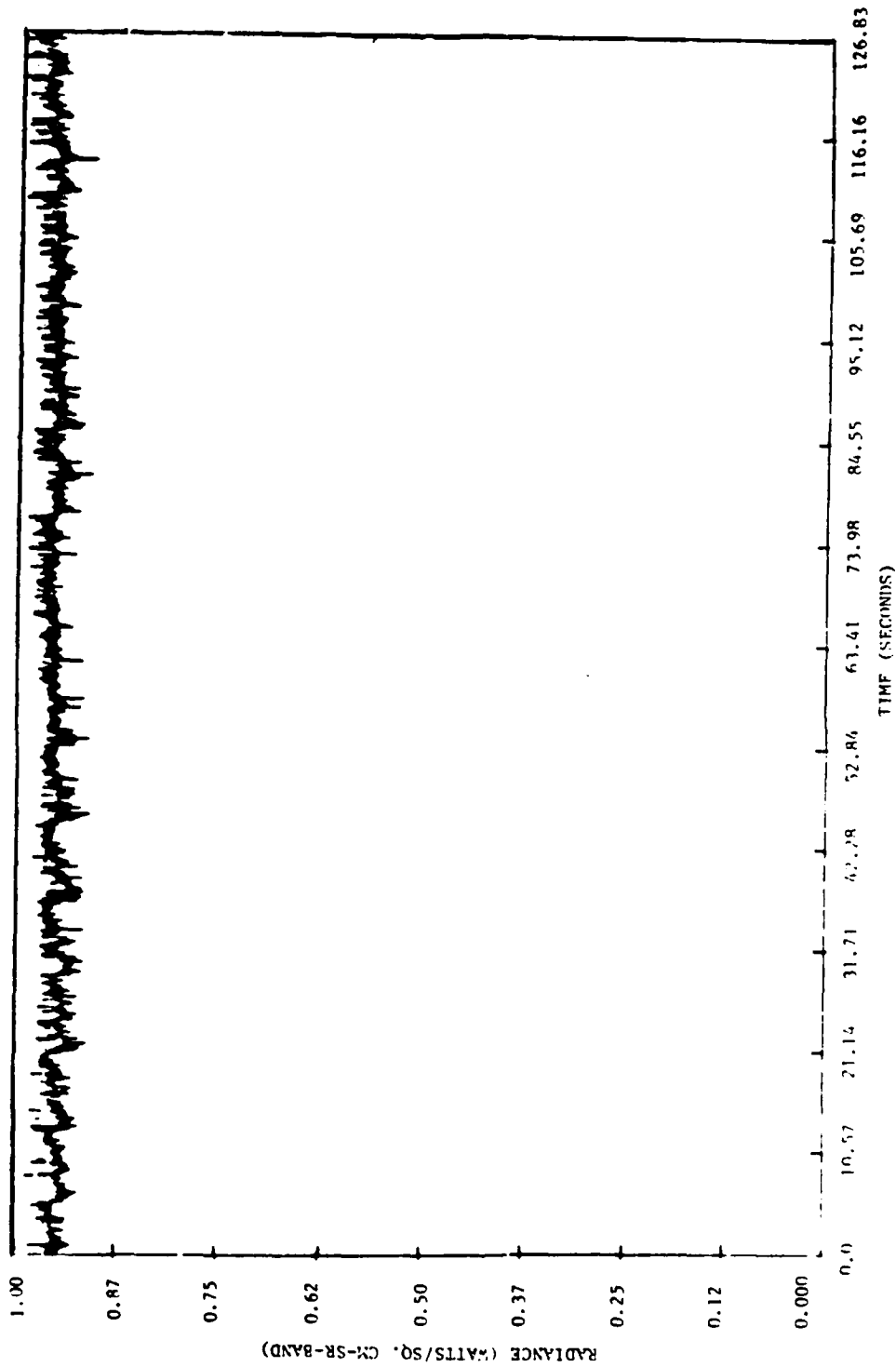


Figure 16. Radiance-Time Profile (24) for a Cumulus Cloud - Clear Air Background (Staring Mode)

## 5. SUMMARY

A model which describes the scattering, absorption, and emission of radiation by atmospheric water or ice clouds has been developed, based on an approximate solution to the radiative transfer equation. The cloud model is combined with the LOWTRAN atmospheric transmission model and can be used to predict the apparent spectral radiance from clouds as detected by a downward-looking observer, including the effects of solar scatter, thermal emission, transmitted upwelling radiation, and atmospheric attenuation. The model is completely general in terms of sun-cloud-observer geometry and applies for clouds of arbitrary optical thickness.

Calculations using the model have been compared with infrared cloud data from several sources. Comparisons with spectral data in the 2.7-2.9  $\mu\text{m}$  and 2.5-6.0  $\mu\text{m}$  regions show generally good agreement in the spectral dependence of the cloud signal, although discrepancies on the order of a factor of two are indicated in the directional dependence (i.e., for solar scattering angles of  $10^\circ$  or less). More detailed comparisons with a larger set of data are required to assess the practical importance of the various approximations in the model.

Comparisons of model predictions with data from the BAMM radiometer test-flight show generally good agreement in terms of predicted and measured terrain background signals. Both the data and the calculations suggest that low altitude cumulus clouds are not an important source of background signal variations in the 2.7-3.1  $\mu\text{m}$  region. More detailed data comparisons, particularly emphasizing spectral radiance, are required to establish the relative magnitudes of low altitude cloud signals compared with the background terrain.

The model calculations illustrate that high altitude cirrus clouds can cause large variations in the upwelling radiation signal in the 2.7-3.1  $\mu\text{m}$

region. The band radiance for background scenes including such a cloud can be several times the clear air radiance, even for an optically thin cloud. This effect arises because the cloud is above most of the atmospheric water vapor, and attenuation of the scattered sunlight is not as severe as in the case of low altitude clouds. An analysis of elevation scan data show that solar scattering from a high altitude cirrus cloud is a plausible explanation for the large IR signal increase associated with apparent haze in BMM Scene Ia. A consideration of potential signal variations from such clouds is likely to be important in the design of downward-looking surveillance systems.

The cloud model discussed in this report successfully describes the background IR signals from different scenes, including both thin and thick clouds. The model provides a useful tool for analyzing and interpreting background scenes observed from the BMM platform. These analyses are important in assessing the upwelling radiances which would be measured from a satellite platform.

## REFERENCES

1. van de Hulst, H.C., "A New Look at Multiple Scattering," Institute for Space Studies Report, NASA, New York (1963).
2. Hansen, James, E. and Pollack, James B., "Near Infrared Scattering By Terrestrial Clouds," J. Atmo. Sci., 27, 266 (1970).
3. Hansen, James E., "Exact and Approximate Solutions for Multiple Scattering by Hazy Atmospheres," J. Atmo. Sci., 26, 478 (1969).
4. Welch, R.M. and Cox, S.K., "Absorption of Solar Radiation in Clouds: The Effect of Monomodal and Bimodal Size Distributions," Third Conference on Atmospheric Radiation, American Met. Soc. (1978).
5. Davies, Roger, "The Three-Dimensional Transfer of Solar Radiation in Clouds," Ph.D. Thesis, University of Wisconsin, Madison, Wisconsin (1976) and J. Atmo. Sci.
6. McKee, T.B. and Cox, S.K., "Scattering of Visible Radiation by Finite Clouds," J. Atmo. Sci., 31, 1886 (1974).
7. Liou, Kuo-Nan and Wittman, Gerald D., "Parameterization of the Radiative Properties of Clouds," J. Atmo. Sci., 36, 1261 (1979).
8. Roewe, Douglas and Liou, Kuo-Nan, "Influence of Cirrus Clouds on the Infrared Cooling Rate in the Troposphere and Lower Stratosphere," J. Appl. Meteor., 17, 92 (1978).
9. Harshvardhan, "Perturbation of the Zonal Radiation Balance by a Stratospheric Aerosol Layer," J. Atmo. Sci., 36, 1274 (1979).
10. Pruppacher, Hans, R. and Klett, James D., "Microphysics of Clouds and Precipitation," Reidel Publishing Co., Boston (1978).
11. Kuhn, P.M. and Weickmann, H.K., "High Altitude Radiometric Measurements of Cirrus," J. Appl. Meteor., 8, 147.
12. Chandrasekhar, Radiative Transfer, Dover, New York (1950).
13. McElroy, M.G., "The Composition of Planetary Atmospheres," J. Quant. Spectrosc. Radiat. Transfer, 11, 813 (1971).

References (Cont.)

14. Friedlander, S.K., Smoke, Dust, and Haze, John Wiley and Sons, New York (1977).
15. Zachor, A.S., Holzer, J.H., Smith, F.G., "IR Signatures Study," Honeywell Electro-Optics Center Report No. 7812-8, December 1978.
16. Shettle, E. (Calculations reported in Zachor, et al., Ref. (15)).
17. Deirmendjian, "Scattering and Polarization Properties of Water Clouds and Hazes in the Visible and Infrared," Appl. Opt., 3, 187 (1964).
18. Liou, Kuo-Nan, "Light Scattering by Ice Clouds in the Visible and Infrared: A Theoretical Study," J. Atmo. Sci., 29, 524 (1972).
19. Henyey, L.G. and Greenstein, J.L., "Diffuse Radiation in the Galazy," Astrophys. J., 93, 70 (1941).
20. Meador, W.E., and Weaver, W.R., "Two-Stream Approximations to Radiative Transfer in Planetary Atmospheres: A Unified Description of Existing Methods and a New Improvement," J. Atmo. Sci. 37, 630 (1980).
21. Bernstein, L.S., Duff, J.S., Stanton, A.C., and Robertson, D.C., in preparation.
22. Wiscombe, W.J., and Grams, G.W., "The Backscattered Fraction in Two-Stream Approximations," J. Atmo. Sci. 33, 2440 (1976).
23. Selby, J.E.A., Shettle, E.P., and McClatchey, R.A., "Atmospheric Transmittance from 0.25 to 28.5  $\mu\text{m}$ : Supplement LOWTRAN3B," AFGL-TR-76-0258, Air Force Geophysics Laboratory, Hanscom AFB, MA 01731 (November 1976). ADA040701.
24. Young, S.J., "Scattering of Solar Radiation by Clouds," The Aerospace Corporation Report TR-0079 (4970-40)-1, December 1978.
25. Espinola, R.P., "Spectral and Spatial Properties of Cloud Backgrounds from 2.65 to 2.95 Microns," Report No. 70505F, Arthur D. Little, Inc., Cambridge, MA 02140 (1970).
26. Sandford, B.P., Schummers, J.H., Rex, J.D., Shumsky, J., Huppi, R.J., and Sluder, R.B., "Aircraft Signatures in the Infrared 1.2 to 5.5 Micron Region. Volume I: Instrumentation," AFGL-TR-76-0133, Air Force Geophysics Laboratory, Hanscom AFB, MA 01731 (1976). ADB014088L.

27. Liou, K.-N., "Transfer of Solar Irradiance through Cirrus Cloud Layers," *J. Geophys. Res.* 78, 1409 (1973).
28. Murphy, R.E., Cook, F.H., Grossbard, N.G., Grieder, W.F., and Yap, B.K., "Balloon Altitude Mosaic Measurements (BAMM) Data Report II," Air Force Geophysics Laboratory, Hanscom AFB, MA 01731 (1979).
29. Wolf, W.L., and Zissis, G.J., Ed., The Infrared Handbook, (Office of Naval Research, Department of the Navy, Washington, DC, 1978).